Marine and Petroleum Geology 105 (2019) 1–16

Contents lists available at ScienceDirect

Marine and Petroleum Geology

journal homepage: www.elsevier.com/locate/marpetgeo

Research paper

Deformation band formation as a function of progressive burial: Depth calibration and mechanism change in the Pannonian Basin (Hungary)

Barbara Beke[a,*], László Fodor[a,b], Lisa Millar[c], Attila Petrik[b]

[a] MTA-ELTE Geological Geophysical and Space Science Research Group, H-1117, Budapest, Pázmány Sétány 1/C, Hungary
[b] MTA-ELTE Volcanology Research Group, H-1117, Budapest, Pázmány Péter Sétány 1/C, Hungary
[c] Department of Civil and Environmental Engineering, University of Strathclyde, Glasgow, UK

ARTICLE INFO

Keywords:
Deformation bands
Deformation mechanism
Depth calibration
Subsidence modelling
Basin evolution
Cementation

ABSTRACT

Deformation bands (DB) are ubiquitous structural elements that can be found in Miocene pre- and syn-rift sediments of the extensional Pannonian Basin, central Europe. Across the field sites we see examples of disaggregation to cataclastic DB sets and evidence of frequent reactivation by discrete faulting. Thin section analysis, cross-cutting relationships and well-defined time constraints of analysed brittle structures demonstrate that with increased burial depth, DB deformation mechanisms progressed from granular flow to cataclasis.

The DB sets were classified into 10 deformation phases based on formerly published independent fault-slip analysis and structural mapping. Subsidence curves were constructed for each stratigraphic level involved in deformation and were used along with the intersection of deformation episodes to calculate the depth intervals of DB generations and subsequent structural elements. The DB formation depths obtained were transferred to the depth range of the related mechanisms. This combined methodology permits a more quantitative approach to determine the changes in the deformation mechanisms with depth.

Our results show that granular flow (disaggregation bands) dominates down to 100–150 m as the earliest deformation structure, followed by weak then moderate cataclasis. The transition between weak and moderate cataclasis is at approximately 300 ± 100 m for host rock rich in feldspar or fragile tuffitic components and from around 900 ± 100 m in quartz-rich sediments. In addition, deformation by frictional sliding concentrates on discrete fault planes at the margin of cataclastic bands or on new fracture planes from ~500 ± 100 m in volcanoclastic or feldspar rich host rocks, and 1000 ± 100 m in quartz-rich host rocks.

We suggest that burial-induced diagenetic processes is dependent on subsidence history, and partly in connection with regional fluid migration path, control the transition from moderate or advanced cataclasis to discrete fault slip. All these changes affect the pore structure and porosity that contribute to rheological changes, and hence change in deformation mechanism of coeval fracturing events.

1. Introduction

Deformation bands (DB) are common tabular strain localization structures (Aydin, 1978) developed in porous, granular sediments. DBs are generally classified by either kinematic features (Aydin et al., 2006) or prevailing deformation mechanism (Fossen et al., 2007). The kinematic features are mainly governed by a (regional) stress field. Starting from the sedimentation interface towards a deeply buried position, the deformation mechanisms change from grain rotation combined with grain boundary sliding (disaggregation band) toward increasing proportion of cataclasis (cataclastic band), then dissolution of grains (dissolution and cementation band). Confining pressure, temperature and tectonic regime are suggested to control the deformation mechanism and the distribution of DBs (Mair et al., 2000; Hesthammer and Fossen, 2001; Ballas et al., 2014; Soliva et al., 2016) as temporally changing factors. However, the main deformation mechanism is generally determined by the petrophysical properties of host rocks (Schultz and Siddharthan, 2005; Balsamo et al., 2008; Fossen et al., 2007, 2017) such as porosity, cementation (e.g., Bernabé et al., 1992), mineralogy (Rawling and Goodwin, 2003), grain sorting (Antonellini and Pollard, 1995), grain size and distribution (Cheung et al., 2012), and roundness (Zhang et al., 1990). Some of these properties gradually change with increasing burial depth in line with confining pressures resulting in compaction and a reduction in porosity. Progressive burial of sediment induces the initiation and development of diagenetic processes, such as mechanical compaction, chemical solution, formation of authigenic

* Corresponding author.
E-mail address: barbara.beke@gmail.com (B. Beke).

https://doi.org/10.1016/j.marpetgeo.2019.04.006
Received 16 August 2018; Received in revised form 3 April 2019; Accepted 5 April 2019
Available online 11 April 2019
0264-8172/

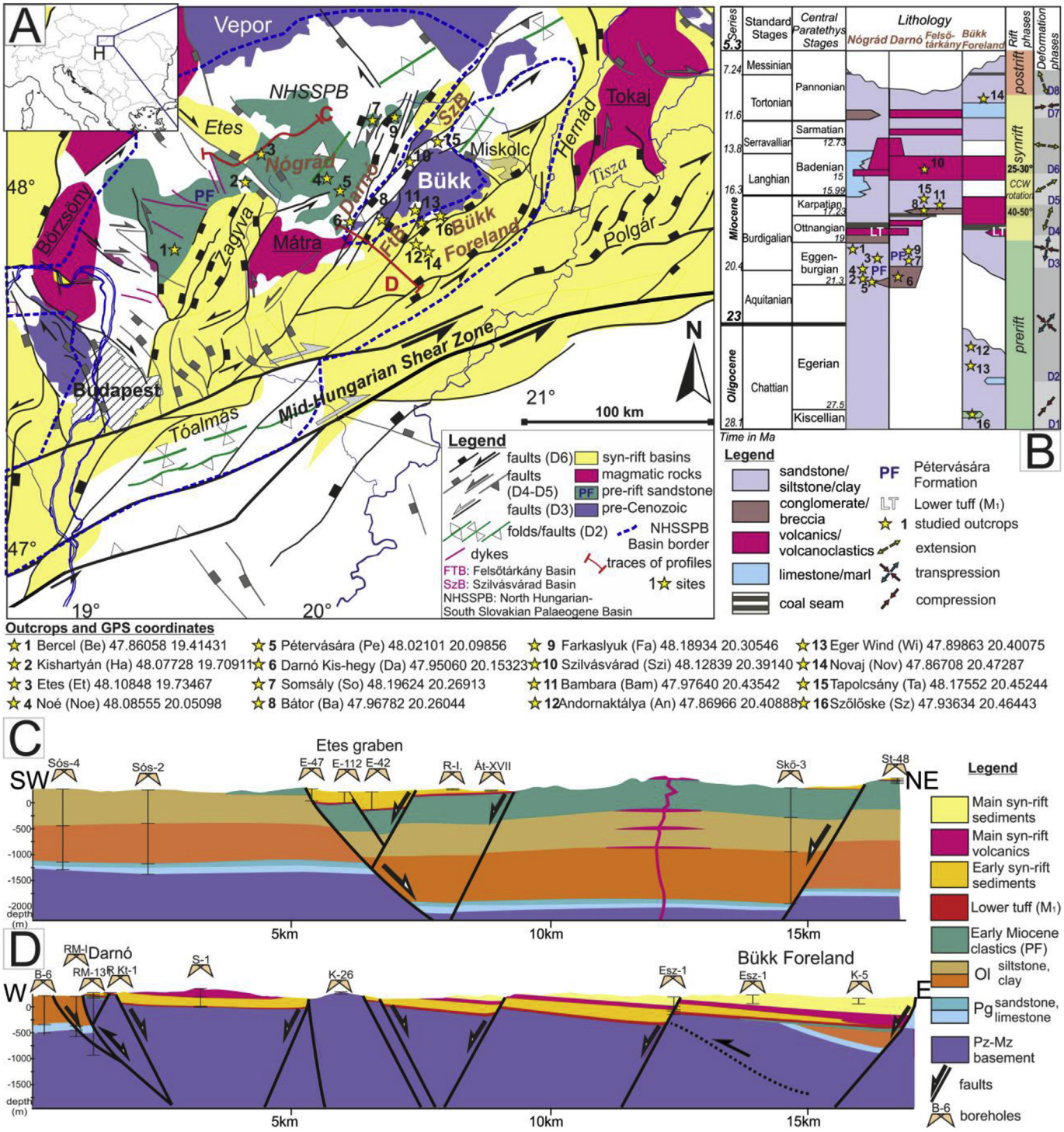

Fig. 1. (A) Simplified geological setting of the area showing the main structures and outcrops. (B) Stratigraphic column of study area with sampling points and tectonic phases. (C) Geological cross-section along the SW-NE direction within the study area (D) Geological cross-section along the NW-SE direction within the study area.

minerals and cementation. This results in more densely packed grains, therefore creating a more consolidated rock. One possible expression of physical changes to host sediments can be at the end of DB evolution where a change to frictional slip along a discrete fault plane is observed, new joints form or mineral-filled veins develop.

Although the depth dependence of deformation mechanisms is generally accepted, there are limited studies which estimate the specific depth interval of band types (Cashman and Cashman, 2000; Davatzes et al., 2005; Fossen, 2010a; Exner and Tschegg, 2012; Hodson et al., 2016). These estimates are mostly based on the calculation of potential thickness of sediment cover. The lack of more detailed interval calibrations is most likely due to several factors influencing the deformation mechanism leaving the crucial timing of DB formation unresolved.

In our earlier works (Petrik et al., 2014, 2016; Beke, 2016) we used subsidence curves in the extensional Pannonian Basin, central Europe to reveal deformation mechanism trends which can be directly related to the burial history. The major goal of this study is to provide a more detailed and precise depth range calibration for different band types

and their associated deformation mechanisms in the Pannonian Basin. For this purpose, multiple generations of deformation bands and other brittle elements were analysed from 16 outcrops, representing 4 sub-areas marked by different subsidence history. The study area is located within the North Hungarian Range, where the 4 sub-basins are exposed due to Plio-Quaternary uplift and denudation. The possibility of finer resolution of deformation mechanism is due to favourable local structural evolution including frequent and rapid changes in the direction of deformation band and fault sets. The finer depth calibration of DB mechanisms may contribute to better understanding the role of distinct type of DBs on regional fluid migration with depth.

1.1. Earlier estimates on depth ranges for DB types and mechanisms

It is widely accepted that deformation mechanism strongly depends on external physical conditions closely connected to the burial path (Engelder, 1974; Schultz and Siddhartan, 2005; Fossen et al., 2007, 2017). Simplified calibration of depth control of DB types was introduced by Fossen et al. (2007); they proposed near-surface to shallow burial formation depth for disaggregation band and divided shallowly (< 1 km) and deeply formed (1–3 km) cataclastic bands with weaker and more advanced cataclasis, respectively. However, few studies considered the subsidence path of the host rock (Fossen, 2010a) or thickness of cover sediments; even in these cases the time of deformation remained less constrained resulting in considerable uncertainty in the depth calibration.

Disaggregation band was mentioned from less than a few hundred meters burial (Torabi and Fossen, 2009). Shallow cataclasis was reported in unconsolidated sand with maximum 50 m formation depth (Cashman and Cashman, 2000). Exner and Tschegg (2012) roughly estimated a maximum of 150 m formation depth (corresponding to ca. 3–5 MPa overburden pressure) for investigated DBs in the Vienna basin. Ballas et al. (2013) presumed 400 ± 100 m covering sediments for shear-enhanced cataclastic bands formation in France. Rawling and Goodwin (2003) calculated 20–30 MPa (~1 km) overburden pressure for shallow cataclasis.

The classical cataclastic bands were only described from deeper burial depth (> 1 km). This type formed at ca. 1.5 km depth in Sinai (Rotevatn et al., 2008) and at 2–3 km depth in the Navajo and Entrada Sandstones (Davatzes and Aydin, 2003). These examples clearly show that the depth range was poorly calibrated due to many uncertain factors, including multiple control points in deformation history.

2. Geological setting

2.1. Main tectono-sedimentary events in the Pannonian Basin

The Pannonian basin is the result of lithospheric stretching which affected the thickened crust of the Alpine-Carpathian-Dinaridic orogenic system (Royden et al., 1982; Horváth et al., 2015; Balázs et al., 2016). The contractional deformation of this orogeny started in the late Jurassic and reached continent-continent collision in the late Eocene (Schmid et al., 2004). In the area of the later Pannonian basin, post-collisional shortening resulted in a series of middle Eocene to early Miocene contractional basins which were formed in the hinterland of the Alpine-Carpathian-Dinaridic orogen (Báldi, 1986; Nagymarosy, 1990; Tari et al., 1993; Vass, 2002). These retroarc flexural basins register broadly NW-SE compression. The study area (Fig. 1A) is located in one of these basins, in the North Hungarian–South Slovakian Paleogene Basin (NHSPB, Fig. 1A) which existed between 35 and 18.5 Ma (Fig. 2A).

The youngest formation of the NHSPB basin fill (and the main focus of this study) was a shallow, tide-dominated marine sandstone (Pétervására Fm., PF) deposited between ca. 21–18.5 Ma (Sztanó, 1994, 1995; Sztanó and Tari, 1993). After deposition, this Early Miocene sandstone was exposed to the surface and eroded between ~18.5 and

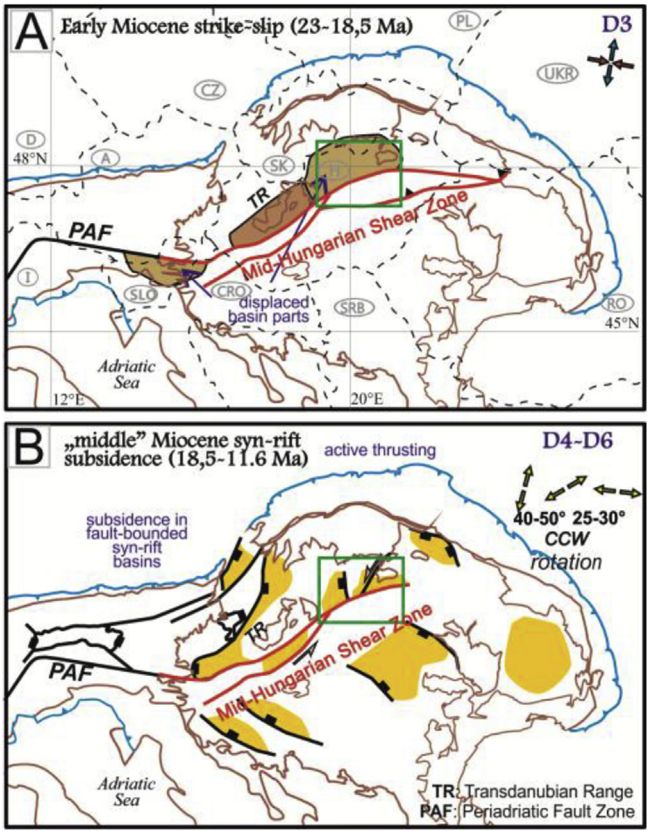

Fig. 2. Geodynamic setting and schematic structural evolution of the Pannonian Basin within the Alpine-Carpathian-Dinaridic orogeny: A) pre-rift and B) syn-rift phases.

18.2 Ma, before the onset of the first syn-rift sedimentation of the Pannonian basin. The pre-rift PF is the key element for the comparative analysis of deformation mechanisms because it hosts most of the sites and records all deformation events; from the last pre-rift to syn-rift phases and post-rift events.

Prior to the Pannonian Basin formation large-scale dextral shearing took place along the wide Mid-Hungarian Shear Zone (Figs. 1A and 2A), which marks the southern boundary of the study area (Csontos and Nagymarosy, 1998). The shear zone is the continuation of the Periadriatic fault of the Alps (Fig. 2) where kinematic and time constraints are also available (Schmid et al., 1989; Müller et al., 2001). The onset of dextral slip is somewhat uncertain, but it is estimated to have taken place between 32 and 28 Ma based on magmatic intrusions along the active fault zone (Blanckenburg et al., 1998; Pomella et al., 2012). Reconstructed paleogeography during the PF deposition (Sztanó, 1994) indicates that the fault zone represented the southern margin of the NHSPB basin (Fig. 1A) in the Pannonian basin area and dextral slip continued from ~21 to ~18.5 Ma (Fig. 2A, Fodor et al., 1998).

The syn-rift deformation and associated subsidence of the northern Pannonian basin started with extensional rhyolitic volcanism at ca. 18.2 Ma, (Lukács et al., 2018). The fastest subsidence, the major faulting phase and continuing volcanism occurred between 17.25 and 12.8 Ma (Karpatian and Badenian; see recent chronological calibrations of Hohenegger et al., 2014; Sant et al., 2017). Syn-rift deformation was connected to two phases of vertical-axis rotation up to 80° in counter-clockwise sense, between ca. 17 and 15 Ma (Fig. 1B) (Márton and Fodor, 1995). The change from syn-rift to basically non-tectonic post-rift phase was traditionally placed at the boundary of Middle to Late Miocene (~11.6 Ma, e.g., Horváth et al., 2015), while new works demonstrated renewed faulting (modest rifting) in the early Late Miocene up to ~9 Ma (Balázs et al., 2016; Petrik et al., 2016).

2.2. Structural setting and stratigraphy of the study area

The study area (Fig. 1A) was entirely located within the NHSPB during the pre-rift evolution and occupied several grabens of the Pannonian basin. Within the NHSPB the Darnó Zone (Fig. 1A,D) represents the most important structural and paleogeographic boundary which influenced the distribution of the sampled Pétervására Formation (PF, Fig. 1A). Both the Paleogene–early Miocene, syn-rift stratigraphy and the fault pattern are slightly different within the fault zone (to the west) and east of the fault zone. In this section we have summarized the evolution of the whole study area as one because the stress field evolution is the same in each of the fours sub-areas: Nógrád, Darnó, Felsőtárkány-Szilvásvárad, and Bükk Foreland.

The earliest D1 deformation phase (Petrik et al., 2014) is mainly characterised by NE–SWcompression, but less typically perpendicular NW–SE extension also occurred (site 16 Fig. 1B) and might have existed from ~28 to ~25 Ma. D2 phase characterised the contractional evolution of the NHSPB, and lasted from ~25 to 20.5 Ma. The upper time constraint comes from site Da (site 6, Fig. 1), which is the youngest rock affected by this deformation (Sr-isotopic age 20.9–21.4 Ma, Less and and Frijia, 2015). Phase D3 correspond to the dextral strike-slip faulting and lasted up to the terminal deposition of the PF at ca. 18.5 Ma. The subsequent D4 phase represents already the onset of the extensional stress field thus the rifting of the Pannonian basin (Figs. 1B and 2B). We place the beginning of D4 phase at the first volcanoclastic level which erupted at 18.2 Ma (Lukács et al., 2018). The other constraint is given by well-documented vertical-axis rotation (Fig. 1B); the first increment of such counterclockwise rotation between the D4 and D5 phases (Márton and Fodor, 1995). New geochronological data on largely and moderately rotated volcanites place this rotation, and therefore the boundary of D4 and D3 phases around 17Ma (Lukács et al., 2018). This is in agreement with stratigraphy (Hámor, 1985), which recorded a change in subsidence around 17 Ma (possibly from 17.2 Ma). D5 phase correspond to the increased subsidence rate, and this important extensional phase terminated with the second CCW rotation at ~15 Ma. During the subsequent D6 phase, extension took place in a ESE-WNW direction (Petrik et al., 2016). This deviated from the early D4 phase of NNE-SSW and was caused by rotation of the entire area. D7 is a short-lived compressional phase, which sporadically occurs in the entire Pannonian basin (Fodor et al., 1999) and can be connected to local erosion of terminal Middle Miocene rocks, it is thus placed between 12.1 and 11.6 Ma (tentative length of 0.5 Ma). D8 phase represents the continuation of syn-rift extension, whose end is locally constrained as 9.7 Ma from combined magnetostratigraphic-seismic data (Petrik et al., 2016). The boundary of post-rift D9 and neotectonic D10 phases is tentatively placed at 6 Ma (Petrik et al., 2016) but is poorly constrained locally.

2.2.1. Nógrád area

We considered all parts of the NHSPB west of the Darnó zone (Fig. 1A), irrespective to structural evolution during the rifting. Oligocene basin fill is composed of fine-grained clastics deposited in shallow bathyal environment. The final basin fill, the PF is widespread, with thickness more than 400 m. Traces of D4 faults were recognized in outcrops only, although the onset of sedimentation (coal seems with marginal marine clastics) would imply the presence of map-scale (50–100 m) faults.

Late early to mid-Miocene syn-rift basin fill sequences are preserved in grabens with variable orientation. The variable fault directions correspond to several faulting phases described above. The NW-SE trending Etes graben formed during the D5 rifting phase, mostly between 17.2 and ~15 Ma (Hámor, 1985), the connected faulting resulted in the fastest subsidence and fine-grained, deep marine basin fill. The Zagyva graben initiated later, where the main subsidence and faulting occurred from 15 to ~9 Ma during the D6 and D8 phases with similar stress axes and fault kinematics. The difference in fault orientation is due to the second CCW rotation. Basin fill was variable, from marine siltstone to marginal carbonates, both interfingering with thick volcanoclastic sequences (Hámor, 1985).

We have studied Early Miocene four moderately consolidated sandstones, and a siltstone at five outcrops in this area (Fig. 1A and B) among them the PF is the most represented.

2.2.2. Darnó area and Felsőtárkány and Szilvásvárad grabens

The western fault branches of the Darnó zone were initiated in the late Oligocene, during D2 phase and remained active during D3 phase. These faults had contractional character; sinistral-reverse and purely reverse during D2 and D3 phases, respectively (Zelenka et al., 1983; Sztanó and Józsa, 1996; Fodor et al., 2005) and form a few km wide thrust zone. Due to these two phases the south-eastern hanging wall of this fault zone was uplifted, Paleogene sedimentation was prevented and the deposition of the PF and connected conglomeratic deltas were restricted to the western fault branches (Báldi, 1986; Sztanó, 1994, Petrik et al., 2016). PF and connected conglomeratic deltas arealso missing from below the Szilvásvárad and Felsőtárkány grabens (Fig. 1 A and B). A general denudation event took place between 18.5 and 18.2 Ma, after that the whole Darnó zone underwent common evolution. The syn-rift sequence started with thin volcanoclastics then coal formation (Püspöki et al., 2009), which passed into shallow marine clastic sedimentation during the D4 and D5 phases (Fig. 1B). The thickness of this sequence is much smaller than in the Nógrád area, Supplementary material 3). After the second CCW rotation, (~15 Ma), thin suites of volcanoclastics and marginal marine deposits formed (Fig. 1B). A unique member of the stratigraphy is the late Middle Miocene andesitic volcanic suite (Pelikán et al., 2005). Parallel to deposition of these formations are the NNE-trending grabens, in the wide Darnó Zone, were formed due to transtensional deformation initiated during the D6 phase (Fodor et al., 2005; Petrik et al., 2016). This phase reactivated the western faults of the Darnó zone as normal faults and initiated new faults in the Felsőtárkány and Szilvásvárad basins.

Poorly to moderately consolidated sandstones, pebbly sandstone, conglomerates, subordinate siltstone and tuff-bearing sandstone were studied at seven outcrops (from which three belong to the Darnó Zone) in this area from Early Miocene to Middle Miocene in age (Fig. 1A and B).

2.2.3. Bükk Foreland area

Oligocene of the Bükk Foreland area is similar to that of Nógrád, but the PF is not present (Fig. 1A). Instead, terrestrial sediments occur with paleosols and probable erosional episodes (Fig. 1B) (Petrik et al., 2016). The rifting of the D4 and D5 phases were associated with complex, thick volcanoclastic sequences (Szakács et al., 1998; Harangi, 2001) which record both CCW rotation events. After 14.2 Ma volcanism ceased (Lukács et al., 2018) and fine clastics were deposited in strongly subsiding grabens (Pelikán et al., 2005). Boundary faults of these ENE-trending grabens had multistage kinematic evolution; sinistral transtensional character in the Middle Miocene (D6 phase) and dip-slip normal kinematics in the Late Miocene D8 phase when subsidence was still important (Fodor et al., 2005; Petrik et al., 2016).

The Late Miocene part of the Pannonian basin fill was preserved only in the southern part of the Zagyva, Felsőtárkány and the Bükk Foreland grabens (Hámor, 1985; Pelikán et al., 2005; Magyar et al., 2013). However, vitrinite reflectance, scattered fission track and (U−Th)/He data (Laczó, 1982; Dunkl et al., 1994, Arató et al., 2019) clearly point out the existence of a sediment cover prior to Plio–Quaternary enhanced denudation.

Poorly and moderately consolidated sandstones, conglomerates, subordinate siltstone were investigated at four outcrops of this area, which represent late Early Oligocene to Late Miocene in age. The age distribution of sampled sediments covers pre-rift, syn-rift and post-rift deformation phases.

3. Methods and concept

3.1. Fault-slip analysis and microscopy

The evolution of fault pattern and related stress fields were established through a series of fault-slip analyses carried out locally and at basin scale (see summary in Fodor et al., 1999, local data from Csontos, 1999; Márton and Fodor, 1995; Fodor et al., 2005; Petrik et al., 2014, 2016). Methodology followed the measurement technique of classical structural field work while stress field calculations were implemented by the software package of Angelier (1984) and Angelier and Manoussis (1980), they were first applied by Bergerat et al. (1984) for the study area. We rejected faults from a given set if misfit angle (the angular difference between measured and ideally fitting striae on the fault plane) passed 25°. The uncertainty of stress axes determination cannot be quantified, but we estimate that it will be equal to or smaller than ± 15° (adding imaginary, but still fitting datum does not cause a larger change in axial directions).

Conjugate, en-echelon or Riedel arrangement of DBs and non-striated fractures helped determine the kinematics and estimate the stress axes based on Anderson's (1951) model depicting the relationship of faults and stress axes. DB surfaces often have variable lineations also used for kinematic determination. We compared the strike, dip angle, apparent separation, measured for DBs and for other fracture types (striated or conjugate faults, joints) observed in volcanites, siltstone or conglomerates, where DBs are not present. This comparison permitted the classification of DBs into deformation phases.

Fault patterns were used at multiple map scales including regional surface and subsurface maps (Less and Mello, 2004; Less et al., 2005; Haas et al., 2010). While the detailed maps have 1:50000 scale, we use the term 'map-scale' for faults with displacement larger than 50 m. Different types of faults were identified on industrial seismic profiles (Tari et al., 1992; Ruszkiczay-Rüdiger et al., 2007) and detailed mapping of such faults were carried out within the Mid-Hungarian Zone (Palotai and Csontos, 2010) in the Bükk Foreland and Polgár areas (Tari, 1988; Petrik et al., 2016). Mapped faults were then compared to outcrop-scale (displacement < 50 m) fault pattern, and established surface kinematics were projected to map-scale (50–1000 m displacement) surface and subsurface faults.

Relative chronology of faults was set using cross-cutting relationships among map-scale and mesoscale structures, and superimposed striae on the same fault plane. We also used tilt test of fractures measured in outcrops to separate elements with respect to a specific tilt event (see detailed description in Petrik et al., 2014). If the symmetry plane of conjugate set of fractures were perpendicular or oblique to the bedding plane, fractures are considered as predating or post-dating the tilt of the layers, respectively. If the age of tilting is known from other data sources, the relative age of fracture formation is also determined.

The timing of a given fracture set was constrained through the age of the syn-tectonic sediments; predominantly from the thickened formations in the hanging wall blocks of normal faults. Extensive sets of stratigraphic data (Hámor, 1985; Báldi, 1986) served for determination of fault timing, undeformed stratigraphical units and syn-tectonic thickened successions. Radiometric ages of deformed volcanic rocks (Lukács et al., 2018) also contributed to dating of fractures while younger volcanic levels contained less fracture sets.

For comparative microscopic analysis single DBs were collected (one exception is A4 of DB cluster). Thin sections were investigated under polarized light, cathodoluminescence and scanning electronmicroscope. For petrographic description Zeiss Axioskop light microscope was applied. Cathodoluminescence (CL) studies were performed using a MAAS-Nuclide ELM-3 cold-cathode CL device on polished thin sections. Amray 1830i type Scanning Electron Microscope equipped with INCA Energy-dispersive X-ray spectrometer was used in secondary electron (SE), backscatter electron (BE) and cathodoluminescent (CL) modes and the Hitachi S-4700, 0.5–30 kV type Scanning Electron Microscope was used to analyse polished thin sections and broken surfaces. Some thin sections were stained with Alizarin Red S and K-ferricyanide to identify carbonate minerals.

3.2. Subsidence modelling

Subsidence curves were constructed for all stratigraphic units containing DBs in order to connect the deformation mechanism of bands to the burial history. Input parameters included formation thickness, depositional depth, paleo-water depth, paleo heat flow, stratigraphic ages, and the length of hiatus, which were derived from paleontological and sedimentological researches (Hámor, 1985; Báldi, 1986; Sztanó, 1994; Pelikán et al., 2005; Less, 2005; Less and Frijia, 2015). These data are provided in the Supplementary Data. The thicknesses of formations were compiled from borehole data; in this step we calculated "average values" from the encountered thickness values. During this calculation we did not consider lower values which could be due to stratigraphic omission across normal faults. We also neglected the highest value which was regarded as an exception due to the strongly tilted segments of the formation which leads to an apparent thickness increase. In sum, we averaged 25% of the highest values for each unit to obtain the average value and rounded. In the Nógrád area, we directly used borehole Sámsonháza (Sh-16a) for subsidence modelling because it is located in the vicinity of studied sites (Ha, Noe, Et).

Geological cross sections were constructed from boreholes (Fig. 1C and D) and surface outcrops to constrain the main Cenozoic structural elements and to estimate eroded thickness of the formations (Petrik et al., 2014). This estimate had to take into consideration potential thinning which could be present in the now-eroded compartment of the half grabens. Erosion mostly affected the youngest Late Miocene suite, but the potential error in the estimation of its original thickness has little effect on our topic as DBs are generally older than the onset of Late Miocene sedimentation. A greater effect could be the underestimation of the poorly constrained post PF denudation. The often used 50–100 m is derived from the fact that angular discordance is very small between PSF and the subsequent syn-rift suites.

Subsidence histories were prepared for "average case" (thickness, hiatus, erosion) for each sub-areas (more details in Supplementary material 3). Calculations were constructed by Petromod v11 1D software of Schlumberger-IES Company (Littke et al., 1994).

3.3. Concept for depth calibration of DB types and mechanisms

In order to determine the depth range of a deformation mechanism, characteristic for a given band set, we used the combined methodology displayed on Fig. 3.

First, subsidence curves were constructed for all DB-hosting stratigraphic levels in each of the 4 sub-areas. Then the intersection of the subsidence curves with the initial and terminal boundaries of recognized deformation phases (Fig. 3.). These intersections give the depth interval where all fractures of a given phase could form in a given formation. Thereafter DB sets were classified into 10 faulting phases by comparing geometries of DBs and other structural elements to determine the depth intervals of all DBs.

In the following, we analysed the deformation mechanism of different DB sets. For some examples, the change in deformation mechanism coincides with the change in faulting phases. In the simplest case a change in mechanism occurred at a change of the faulting phases, thus depth and time ranges are the same for phase and mechanism of the DB set (Fig. 3, phase D2, unit A, mechanism 2). However, there are also DB sets where the change in deformation mechanism occurred during the evolution of the band set (D3 of unit B on Fig. 3).

Obviously, formation depth of deformation elements of the same phase varies with the age of the affected formations (D2 phase, units A and B on Fig. 3). This depth difference also reflects changes in deformation mechanism (mechanisms 1 and 2 for D2). On the other hand,

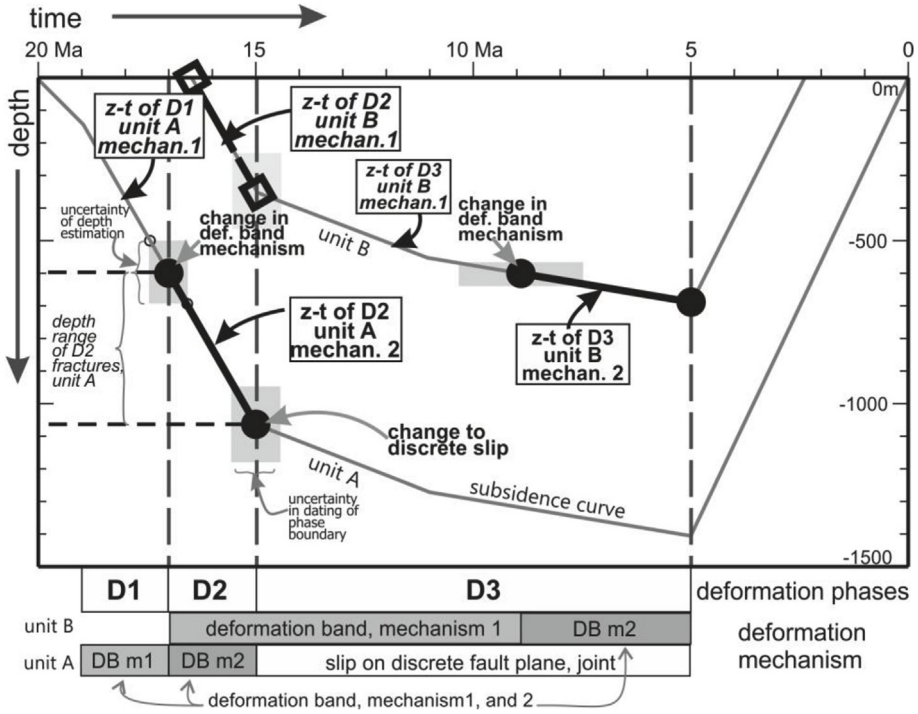

Fig. 3. Concept for the determination of deformation mechanism based on the deformation phases and burial history. Deformation band (DB) formation mechanism changed during phase D3 for the younger unit B, thus depth range of this change has temporal uncertainties shown as wide error box.

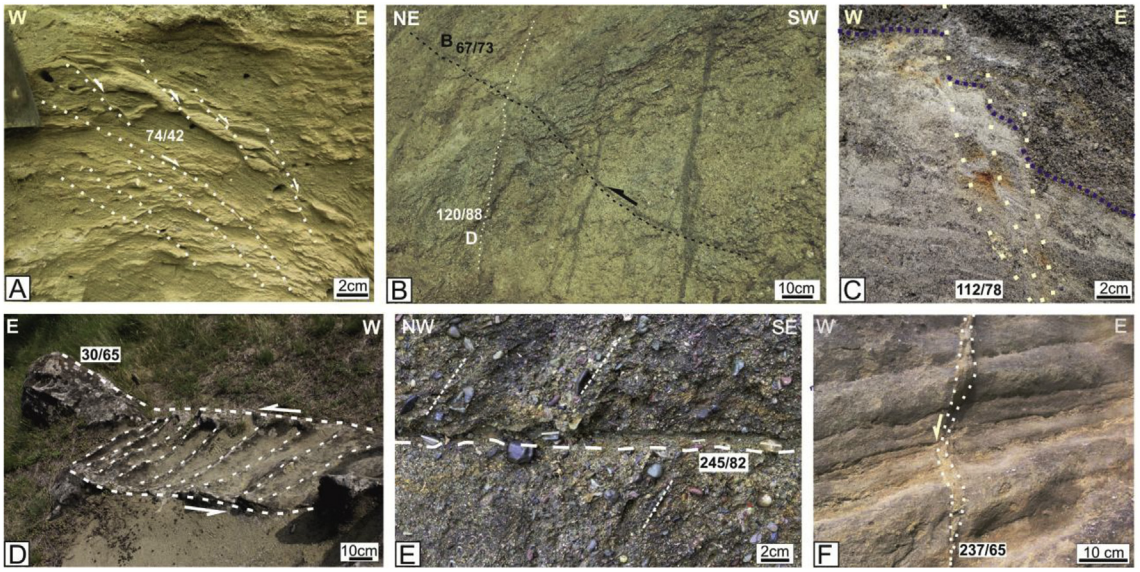

Fig. 4. Field views of different type of deformation band starting from the earliest structures. (A) Tiny DBs (dotted lines) from a lower part of Ta outcrop. These deformation structures are sub-mm thick single DBs along which alternating layers of consolidated sand and-silt are dragged and displaced by several mm to a few cm. (B) Crosscutting relationships of two sets (D is white dotted line and B is black dashed line) of DBs in conglomerate of Da site. 'B' band generation consistently cuts the 'A' and 'D' band generations. The visible displacement is sinistral. (C) Tiny DBs (white dotted lines) show few cm scales offsets on the boundary (dark dotted lines) of finer grained sandy and overlying gravelly, coarse grained sandy units in Ba outcrop. (D) Conjugated DBs (dashed lines) accompanied by massive calcite cementation show strike-slip geometry (R-R′ structures) in pebbly sandstone at So site. (E) Another generation of DB at Da site has strong negative relief. In this single DB grain size is visibly smaller and some intact clasts are oriented parallel with the DB wall (along thicker dashed line). The original orientation of the clasts is marked by thinner dashed lines. (F) Single DB of Ha (contoured by dotted line) has a few cm's displacement.

the same deformation mechanism could occur within markedly different time interval and fracturing phases depending on host formation ages (mechanism 2, phases D2 and D3).

Fig. 3 shows simplified burial history and represents an idealised methodology to calculate the formation depth of deformation element. Uncertainties derive from age determination of faulting phases, (both at the onset and termination), stratigraphic position of sites in the formation, unit thickness, water depth, and finally from the fact that mechanism boundaries do not necessarily coincide with faulting phase boundaries.

Uncertainties in the assumed stratigraphic position are marked by a 50 m thick strip centred around the sites (central line). The maximum depth-time ranges of a given type of DB are shown by a box (Fig. 3). Combination of depth-time ranges from different DB examples results in

a maximum range and an averaged depth interval of a given DB type.

4. Results

First we present the observed brittle structures according to their type and associated deformation mechanism, and then we demonstrate their classification into deformation phases. Then we integrate the type and time constraints of each deformation element into subsidence models in order to calculate depth range of associated deformation mechanism.

4.1. Dilational band

Found at the site Wi of the Bükk Foreland area and developed in Late Oligocene sandy sediment (photos of all studied DB can be found in Supplementary material). The Wi-5 band is characterised by enlarged pore space formed by grain displacements and filled by a fine-grained sedimentary matrix. Calcite fibers have grown in the orientation of dilation which is perpendicular to the band wall. The possible intraformational origin of the matrix (Petrik et al., 2014) suggests they have formed during syn-sedimentary deformation.

4.2. Disaggregation band

Disaggregation DB's are represented in 8 localities (Figs. 4 and 5). Thin section views of mesoscopically individual bands (Fig. 4A and B) show the dominant mechanism is grain reorganization with grain rotation and granular (non-destructive) particulate flow (Fig. 5A, B, C). In partially cemented host rocks, the DBs are cemented with calcite or ferruginous cement (Noe-1, Da-1, Sz-4, Bam-1).

4.3. Cataclastic band

Cataclastic bands are the most abundant DB type in the study area. While the accurate quantification of cataclasis is purposely not the aim of this study, we use a qualitative approach for comparison of the intensity of cataclasis: weak (1), moderate (2) and advanced (3).

In weakly cataclastic bands, roughly intact host rock (‘main’) grains are the prevailing and only a minor amount of matrix is forming during friction. Grain breakage is more abundant among volcanic fragments, calcite and feldspars due to their good cleavage and fragility. More rigid quartz was preferably deformed by abrasion or grain flaking (Rawling and Goodwin, 2003). The remaining pores were frequently filled with cement. Moderate and advanced cataclasis are applied when significant grain-size and porosity reduction are associated with deformation. While in moderately cataclastic bands matrix is mostly derived from strongly comminuted weaker grains (volcanic fragments, calcite and feldspar in order of grain strength), in advancedly cataclastic bands disintegrated quartz grains also form a significant part of the matrix.

4.3.1. Weakly cataclastic bands

The deformation is mainly restricted to grain contacts and rigid grains remain nearly intact (Fig. 5D,E,F). The minor amount of matrix is derived from the most fragile grains (Fig. 5D) or easily deformable phyllosilicates. These bands (Fig. 4C and D) occur as single or anastomosing bands in 10 localities, 4 of which are in pre-rift PF sandstone (Figs. 4D and 5D,E). Although porosity across the DB's was reduced (Fig. 5D,E,F), pores remained large enough for posterior calcite (Fa, So see Figs. 4D and 5D) or ferruginous (Bam, Sz, Ta) cementation (see in Supplementary material 2).

4.3.2. Moderately cataclastic bands

Intragranular fracturing is the dominant grain breaking process among the volcanic-derived fragments (glass), calcite and feldspars. The matrix is fine-grained primarily consisting of the broken fragments of volcanic glass (Fig. 5G) and feldspars. In contrast, quartz grains remained intact, but abraded and are seen to float in the matrix (Fig. 5G and H). Porosity reduction is pronounced resulted in posterior cementation along the outside of the DB. This type occurs in 6 sites (see Fig. 8) as a single (Fig. 4E) band.

4.3.3. Advancedly cataclastic bands

This group contains DBs with significant amount of disintegrated quartz grains as the part of the comminuted matrix material. Few abraded quartz grains were still recognizable in the very fine-grained matrix. The lack of posterior cementation within band is characteristic of the pronounced porosity reduction and the texture resembles cataclastic flow (Fig. 5I). This type occurs in 3 sites (Figs. 4F and 8).

4.4. Types of lineation

Three types of lineations are used to identify kinematics and to give relative chronological constraints on different mechanisms. Several DB surfaces show specific green-coloured lineation where grains seem to be elongated parallel to the slip direction (Fig. 6A). The lineated surfaces generally occur in DBs with high phyllosilicate content, mostly in glauconite or chlorite-rich PF sandstone. SEM - SE images (Fig. 6B) revealed that the lineation consists of alternation of smeared phyllosilicate minerals, predominantly chlorite and rigid grey/light coloured minerals, with quartz. The clay minerals form gentle troughs with sharp cuspate edges indicating ductile behaviour. In this case, lineation appears connected to weakly or advanced cataclastic bands (sites Fa, So, Ha, Noe).

The other type of lineation is composed of calcite fibres (Noe, Da, Fa) which generally occur in small pull-apart style dominoes. Finally, the third type of lineation occurs as sharp grooves on fault surfaces; we refer to as a scratching-type lineation. We consider that these types of lineation formed in the already cemented part of host rock can be connected to frictional slip along discrete fault planes. The location on boundary surfaces of DBs and frequent oblique plunge corroborates their late timing with respect to DB formation and is in line with the change in mechanism from cataclastic flow to frictional slip. Lineation occurs on a clay smear-like film of evolved slip plane at DB cluster of a site. Similar lineation is present in clayey-silty layers of Ba, Pe, Ta sites. The latter three examples demonstrate that low porosity of host sediment has a strong impact on the deformation mechanism therefore relative chronology with respect to DBs cannot be applied to these examples.

4.5. Calcite veins

In Noe and Da sites calcite-filled fractures and advanced cataclastic bands alternate along the same structure. Calcite partly occurs as several mm thick dominoes or as few mm thick veinlets (Fig. 6C) between visibly cataclastic band segments. At site Noe some veins (dominoes) crosscut a well-cemented section of the host sandstone while they continue as deformation bands in less cemented rock. This field evidence suggests that advanced cataclastic bands formed coeval with calcite veining.

4.6. Discrete striated fault planes and joints

In 8 sites deformation band formation was followed by the formation of discrete fractures (sub-mm thick) (Fig. 8). The coexistent DBs and discrete fractures planes in the same lithology reflect the physical changes of host sediments, which ceased further DB evolution. This type of deformation requires consolidated rocks to develop. In cases of band reactivation, younger deformation is concentrated along a very thin zone, asymmetrically on one side of the band (An, Fa sites). Along this boundary surface clay film bearing striations were developed due to clay smear at site An. In cases of Fa, Da sites, oblique lineation with calcite fibres and steps indicate reactivation in a different stress field

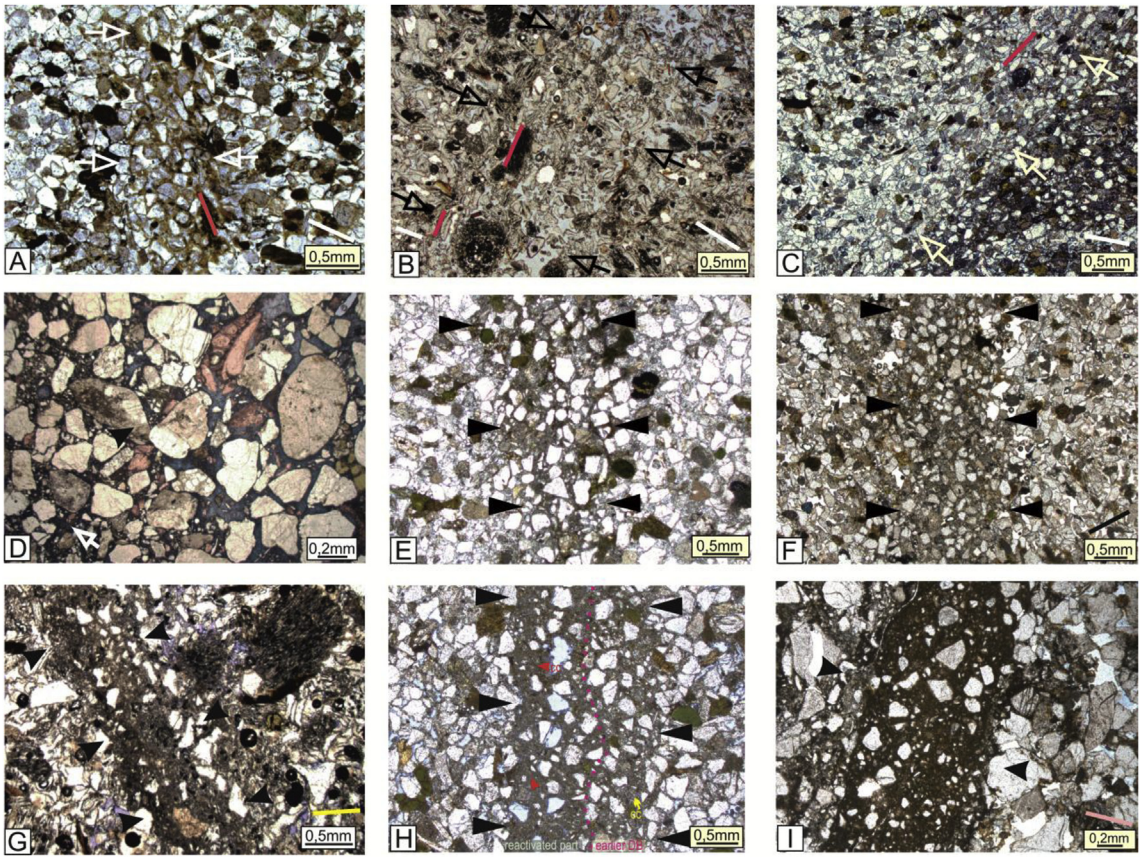

Fig. 5. Transmitted light microscopic views of distinct type of deformation bands. The pale blue color represents the pore space except in D. In D blue represents stained calcite. Sedimentary bedding is marked by white or black continuous lines at the bottom right corners of the pictures of thin sections prepared in a vertical orientation. Red line indicates (re)orientation of grains in disaggregation bands. (A) Disaggregation band (Bam-1) is characterised by zone of reoriented grains without grain fracturing. The pores were filled by yellowish brown cement in the DB. (B) Granular flow is dominant in disaggregation bands of volcanic fragment (glass) rich tuffitic sandstone (Szi-3). (C) At (Ta), outcrop scale synsedimentary deformation is manifested by grain reorganization and rotation without grain comminution in the porous sandstone along the juxtaposition of layers with different porosity. (D) A closer view of typical weakly cataclastic band from So outcrop. The dominant process is grain breakage, but mainly by flaking or chipping of grains. The host rock grains are still recognizable and minor amount of matrix are present. Pores in the vicinity of the DB are entirely filled by blue stained calcite. (E) Fa-1 sample of DB mainly comprises of fragmented feldspar grains and deformed phyllosilicate minerals as matrix, while quartz grains remained nearly intact. The remaining pores filled with calcite cement (greyish color in this photo). (F) In the weakly cataclastic band of Ta-2 sample, only minor amount of matrix and brown cement were observed between 'main' grains. (G) In moderately cataclastic band of Szi-2, grain comminution is pronounced within fragile volcanic components, but a few mechanically stronger grains are still recognizable. (H) In outcrop scale an obliquely reactivated DB shows asymmetrical built up. Calcite microspar cemented (yellow arrow) earlier DB can be seen on the right side of the deformed zone in the photo. On the left side, comminuted (finer grained than in DB on the right side) calcite cement (red arrow in photo) represents the majority of fine grained matrix. (I) Advancedly cataclastic deformation band of Ha shows intense grain size (including quartz) and porosity reduction comparing with the host rock. (I) In the sample of Szi-2 grain comminution is pronounced within fragile volcanic components, but few mechanically stronger grains remained nearly intact. (For interpretation of the references to color in this figure legend, the reader is referred to the Web version of this article.)

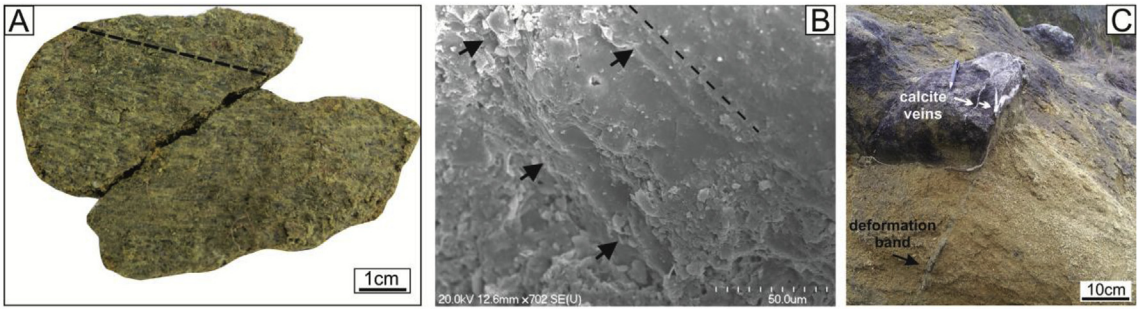

Fig. 6. (A) Field views of phyllosilicate lineation on DB surfaces at Noe site. (B) SEM - SE images of lineation. Black dashed line indicates the orientation of elongation. (C) Field view of calcite veins (white arrows) in the cemented part and coexisting deformation band in the poorly cemented part (black arrow) of PF sandstone at Noe site.

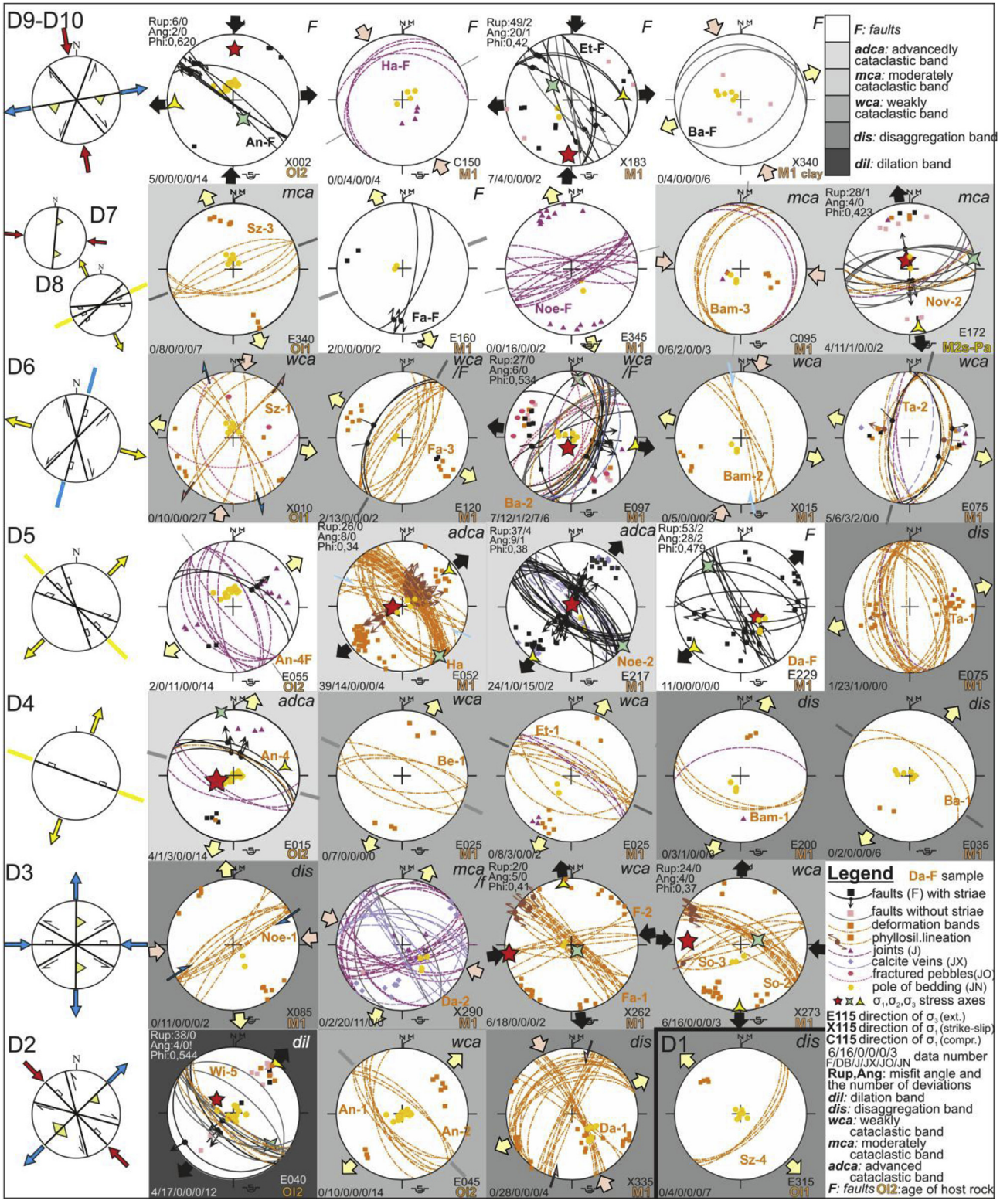

Fig. 7. Stereograms of the observed deformation bands and other brittle elements. Left side column indicates simplified fault pattern and stress axes except for D1 phase (compare Fig. 1B for timing). D1 phase is separated by grey lines from stereograms of other phases. Background color indicates deformation mechanism. (For interpretation of the references to color in this figure legend, the reader is referred to the Web version of this article.)

and deformation mechanism. When kinematics of the band and the fault are the same, the type of lineation is distinct; phyllosilicate lineation is considered as part of band formation, while scratching lineation indicates shear on a discrete fault plane. In sites Pe only this type of lineation occurs, because of the clayey-silty lithology. In some sites new fractures formed as discrete planes (An, Be, Da, Et, Ha, Noe), often associated with scratching-type lineation. Formation of these structures implies a different deformation mechanism from DBs.

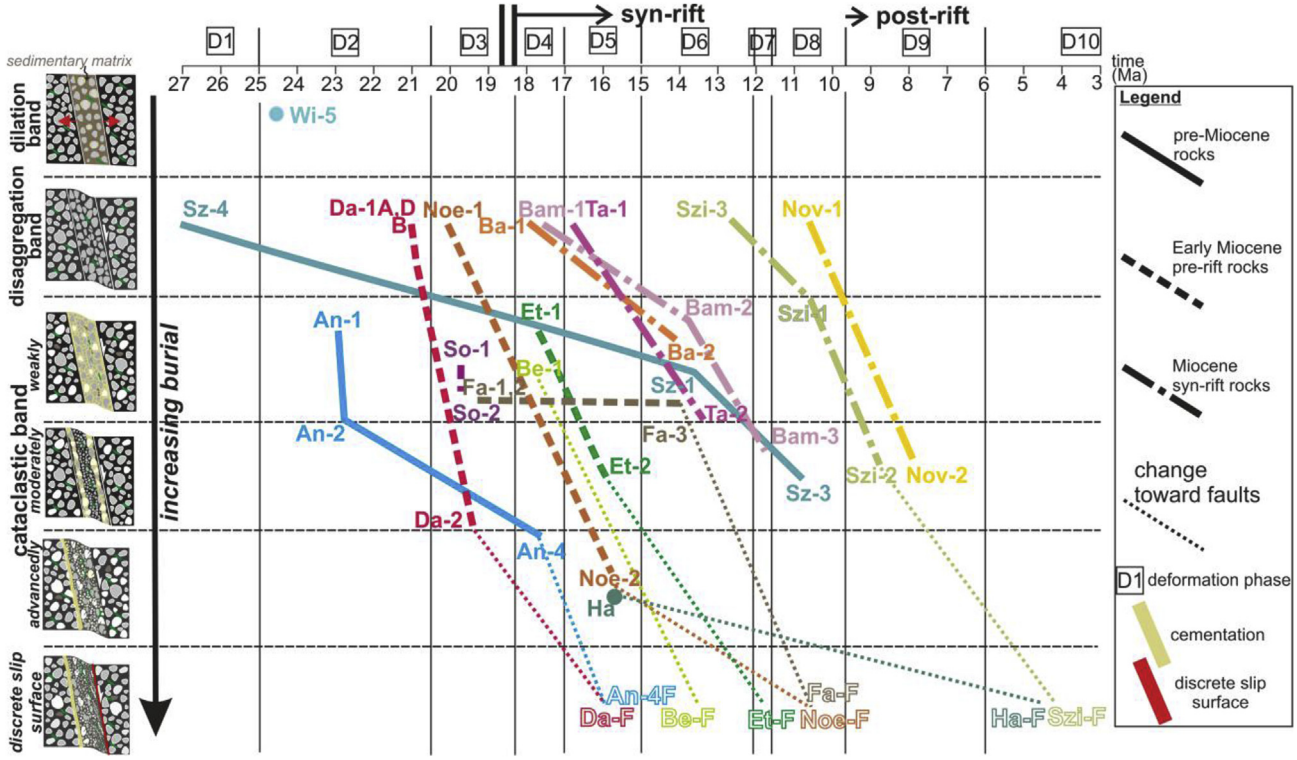

Fig. 8. Deformation mechanism as a function of deformation phases and burial shows clear trend toward faulting.

4.7. Geometry, stress field, and timing of deformation band sets

In this chapter we briefly present the classification of DBs and other structures through the distinct deformation phases D1 to D9 (Fig. 7) (for more detailed description and complete dataset please see Supplementary material 1).

The oldest NE-SW trending DBs occur only in the oldest sampled site (Sz). The tilt test suggests a classification into a separate D1 phase (Fig. 7), not a later phase with similar stress axes.

D2 deformation phase is represented by NW-SE striking bands of normal kinematics including a syn-sedimentary dilation band at site Wind and pre-tilt weakly cataclastic bands. While at site Darnó, deformation resulted in gently dipping NE-trending seemingly reverse and NNE- and NW-striking sub-vertical bands (Da-1 generation); the latter bands have sinistral and normal kinematics, respectively (Fig. 7).

A set of conjugate E and NW-trending DBs belong to D3 phase (Fig. 7). At site Noe, only one sub-vertical set is present, however, because of their geometric similarity to other sites and lack of detected vertical displacement, we consider them to also have a strike-slip character. Some deformation bands (Fa, So) have weak horizontal phyllosilicate lineation on boundary surfaces. Finally, one site (Pe) reveals similarly oriented discrete strike-slip faults in the clayey-silty lithology which correlates to PF. Most of the DBs studied from D3 phase are cataclastic, the only exception are the disaggregation bands from Noe.

The D4 phase, unlike D3, is extensional in character (Fig. 7). Conjugate sets of WNW-ESE trending extensional structures deformed pre-rift, and the earliest syn-rift sediments, thus the D4 phase represents the initiation of rifting. Cataclastic DBs were observed in the oldest sediments while the disaggregation DBs are restricted to the youngest sediments of the D4 phase. One of the disaggregation bands at site Ba-1 is indicative of syn-sediment deformation. Among cataclastic DBs at site Et we have relative chronology based on cross-cutting relationships and the tilt-test: older conjugate DBs formed before the tilting of the host layers.

The D5 phase is characterised by NW-SE trending structures and has a large regional significance, because they developed during the main rifting phase of the Pannonian Basin (Fodor et al., 1999). These structures were mostly formed by NE–SW extension, with slight deviation to ENE–WSW (Fig. 7). In pre-rift sediments (An, Et, Da, Ha, Noe) conjugate normal DBs show the strongest cataclasis developed in the D5 phase. On the surfaces of some bands phyllosilicate lineation indicate normal kinematics. At the site of Ta, syn-rift sediments contain disaggregation bands (Figs. 4A and 5C) of syn-sedimentary character (Beke and Fodor, 2014). Reactivation of DB surfaces by oblique fibre or scratching type lineation (site Da) or lineation on clay smears (site An) is frequent.

Various deformation elements with strike-slip and normal kinematics could form in transtensional setting of D6 phase which is characterised by E − to SE-oriented extension (Fig. 7 and Supplementary 1). Conjugate pairs of weakly cataclastic bands with N−S to NNE–SSW orientation deformed both pre- and syn-rift deposits (Fig. 7). At site Ba, pebbles in the gravelly layers show systematic fracturing parallel to DBs and sharp striated faults in clayey-silty lithology. All these structures correspond to a younger rifting event (syn-rift phase 2).

N–E trending reverse faults of two sites characterise the D7 phase, additional sites were documented by Petrik et al. (2014). In the syn-rift sediments of site Bam N−S trending moderately cataclastic bands with reverse kinematics displaces the two earlier band sets (Fig. 7).

The D8 phase consists primarily of ENE–WSW trending extensional structures (Fig. 7). Cataclastic DBs are present in the oldest (Sz) and the youngest Late Miocene sediments of site Nov (Supplementary material 1). At site Fa, the calcite fibre lineation of D8 reactivated with oblique slip the pre-existing DB planes (D6 phase).

D9 phase indicates ESE–WNW extension and characterised only by discrete faults and joints. Finally, in phase D10 we saw discrete friction-related shear fractures (Fig. 7); NW-trending dextral strike-slips, and few ENE-WSW striking reverse faults which belong to the Plio-Quaternary transpressional neotectonic phase (Horváth, 1995).

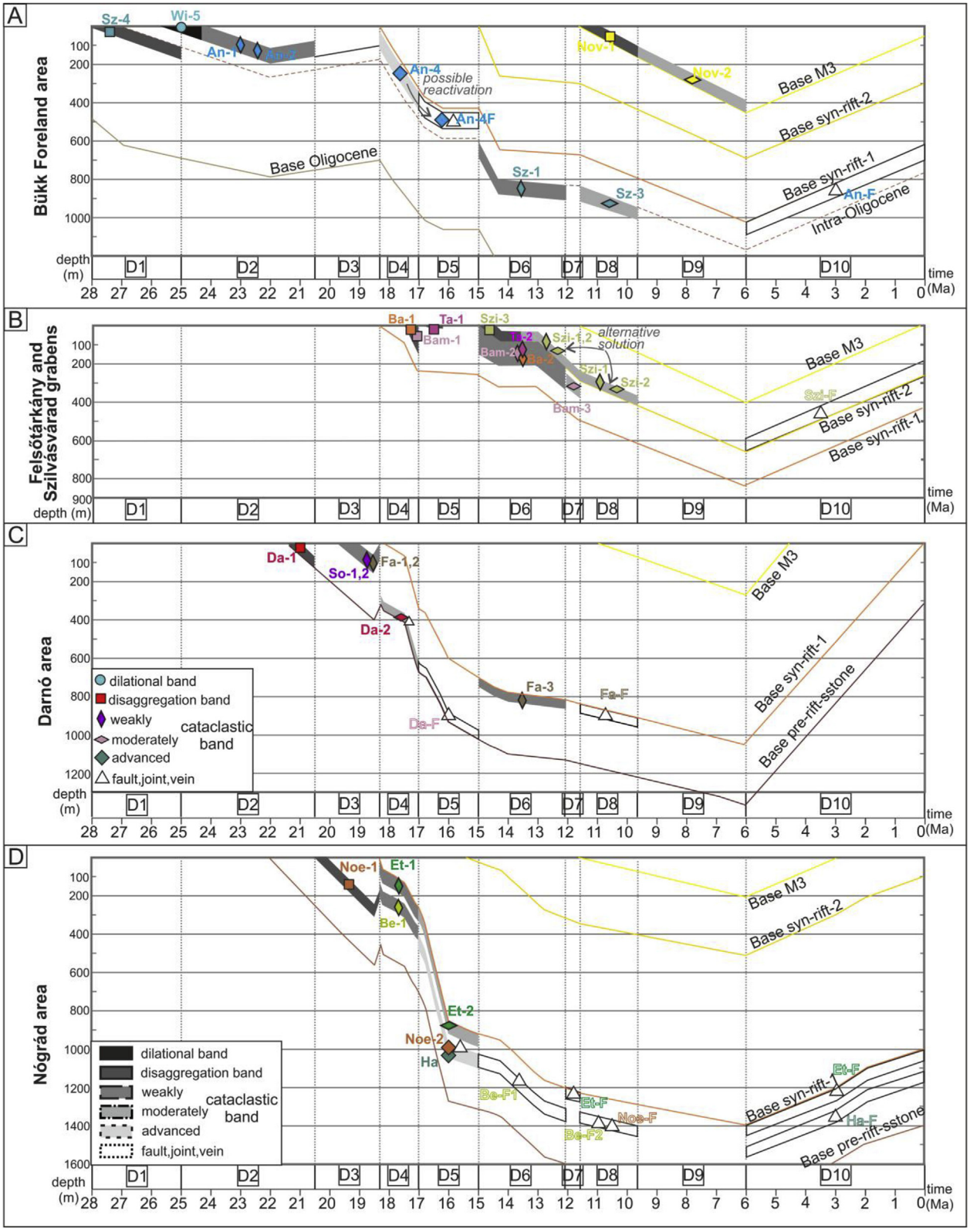

Fig. 9. Estimated depth range of deformation mechanisms as a function of burial and faulting history. Lines correspond to specific horizons; base M3: horizon at the base of Late Miocene; base syn-rift-2: base of sequence of 15–11.6 Ma; syn-rift-1: base of sequence of 18.2–15 Ma. Note uplift and erosion between D3 and D4 phases.

4.8. Depth ranges of DB types and their deformation mechanisms

The correlation of deformation mechanism (see the trend in Fig. 8), deformation phase, deformation time and burial with the independent temporal calibration of deformation phases permitted us to place the formation of each deformation band set into a depth interval following our methodological concept in Fig. 3 (Fig. 9).

4.8.1. Bükk Foreland area

In this sub-area we reconstructed the subsidence history of three

Oligocene and one early Late Miocene site (Fig. 9A). The syn-rift grabens were filled exclusively by volcanic rocks, which show fast accumulation during phases D4 and early D5 followed by a stasis during the late D5 phase. The early Late Miocene was also marked by fast subsidence.

Only one DB generation of dilation band (Wi-5) is supposed to have formed near the surface. Disaggregation bands are represented by two almost synsedimentary generations (Sz-4 and Nov-1) that could have formed between 0–175 m and 0–150 m (Fig. 9A). These two bands constrain the formation of disaggregation type to 0–150 m. While weakly cataclastic bands at site A are constrained to almost the same range (0–200 m), we assume that transition between disaggregation and weakly cataclastic bands could occur around ~150 m depth. However, the clustered deformation bands of An-4 could have already formed between 75 and 425 m.We suggest that the intensity of cataclasis may have evolved progressively during the subsequent phase (375–525 m) of reactivation. The existence of weakly cataclastic band suggests that they formed at the deeper part of given depth interval.

Site Sz shows a different depth ranges for mechanisms; 600–900 m for weak and 825–1000 m for advanced cataclasis (Fig. 9A). This difference can be attributed to the different lithology of quartzite rich gravel, pebbly sandstone.

4.8.2. Felsőtárkány and Szilvásvárad grabens

These two small grabens share similar subsidence history. The syn-rift sedimentation rate was relatively slow during the D5 and slightly accelerated during the second syn-rift event of the D6 phase. Minimum estimate of 400 m Late Miocene cover can be deduced from the Felsőtárkány graben, where it is partially preserved.

All 4 localities provide information on depth range for disaggregation bands; the syn-sedimentary character indicates practically zero but no more than 125 m burial depth at site Bam (Fig. 9B). At site Szi the classification of DBs is somewhat difficult; disaggregation band Szi-3 can be put into early part of D6 phase while Szi-1 weak and Szi-2 moderate cataclastic bands might have formed during the late D6 or D8 phases (see Supplementary material for fracture classification). The derived depth range for disaggregation is 0–75 m in agreement with other sites.

In three rift-related sedimentary sites weak cataclasis is well constrained between 50 and 325 m (Fig. 9B). Depending on the phase classification of Szi-1, -2 bands, weak and moderate cataclasis could occur between 50 and 225 m or 250–425 m. Although they could have formed in the same phase, the kinematics is different. Szi-1formed first and has normal slip character, while Szi-2 formed later and displays a strike-slip character. Meanwhile at Bam the moderate degree of cataclasis could occur at 250–375 m depth.

Striated faults, veins and joints of these sites occur in volcanic tuff (Szi) where DBs are crosscut by joints formed in wide depth range of 250–675 m (Fig. 9B).

4.8.3. Darnó area

Three sites (Fig. 9C) are located along the western boundary of the Darnó Zone. During the D3 phase, these sites were part of the thrust zone, thus pre-rift sandstone thickness is less in comparison to the Nógrád area. Site Da is at the lower end of the PF boundary whereas sites Fa and So are near the upper PF boundary.

Disaggregation bands of Da were formed at shallow depth of 0–125 m shortly after sedimentation. Weak cataclasis of sites Fa and So could occur from the surface down to 175 m depth (Fig. 9C). However, the lower depth boundary could be larger if we underestimate erosion following D3 deformation phase. Moderate intensity of cataclasis of Da-2 could occur in depth interval of 375–675 m. Here calcite dominoes are incorporated with DBs, therefore heterogeneous mechanism could be present along the structure. Striated faults of D5 phase indicate frictional slip in 625–1025 m depth interval, similarly to site Fa-3 (875–975 m, D8 phase, Fig. 9C) with oblique reactivation of DBs. Altogether Da-2 bands and faults at Da sites constrained the depth interval for the transition from DB formation to fault planes at around 625–675 m. In these cases, burial diagenesis-induced petrophysical changes play an important role in the rapid change of deformation mechanism. Weakly cataclastic bands Fa-3 could form between 700 and 875 m and are recorded near the same mechanism of DB formation as sets Fa-1 and Fa-2, although the formation depth intervals are markedly different. A possible explanation could be the rigid quartz-dominated composition of the host rock where the cataclasis does not significantly affect the quartz (only abraded quartz, see Fa-3 in Supplementary 2) above ~ 800 m.

4.8.4. Nógrád area

This area is marked by the fastest syn-rift subsidence (Fig. 9D). Because most bands were formed during the rifting phase, the formation depth of these bands has wide uncertainty in the interval of rapid subsidence. The disaggregation bands at the Noe site could have formed at any depth up to 300 m. Using the subsequent weakly cataclastic bands of Et and Be we can constrain this depth slight more to between 75 and 375 m (Fig. 9D).

From our observations and calculations we can only give a broad range of 250–975 m for the depth at which the gradual increase of cataclasis from weak to moderate degree occurs. The depth interval of advanced cataclasis at Ha and Noe is equally widely constrained between 375 and 1100 m and largely overlaps with the range for moderate cataclasis. Thus estimation of a transition zone is very difficult with the possible difference in depth at the central age of the D5 phase is 875–1000 m. Taking into account all four sites, a wide range of 925–1450 m depth of formation can be suggested for observed discrete faults and joints. The overlap with advanced cataclasis is between 925 and 1100 m, and can be considered as the transition zone of the two mechanisms.

5. Discussion

5.1. Uncertainties for depth range determination

In our contribution we present a quantitative approach to constrain depth intervals of diverse deformation mechanisms of DBs and the change from DB to discrete faults, joints, veins. Our concept has several uncertainties influencing our depth range estimations. We cannot exclude error(s) in the classification of faults and the reconstruction of the evolution. However, the great number of consistent data minimizes this effect. Time of faulting phases rely on precision of stratigraphic data. Although refinements are continuously published (Sant et al., 2017), these generally do not change the boundaries of a phase with more than 0.5 Ma. Such a change can modify the depth range of faults by 100–200 m, and can reach a maximum error of 300 m in the fastest subsiding grabens (Nógrád).

Despite the number of uncertainties in determining the range of depths at which deformation mechanisms occur, we consider that the compilation of similar databases would lead to a quantitative characterisation of the depth of deformation mechanisms – including local petrophysical properties, subsidence and diagenetic histories, heat flow variations influencing rock rheology, and fault kinematics.

5.2. Temporal relationship and depth intervals of deformation mechanisms

5.2.1. Dilation and disaggregation bands

One dilational and several disaggregation bands indicate unconsolidated state of host sediments during the deformation. The time span of deformation phase, under which disaggregation bands formed overlaps with the deposition time of the host sedimentary unit. Our calculations for site Ta show that only a narrow time span elapsed between sedimentation and deformation; less than 1 Ma syn-sedimentary. Larger estimated time spans occurred when DB formation was

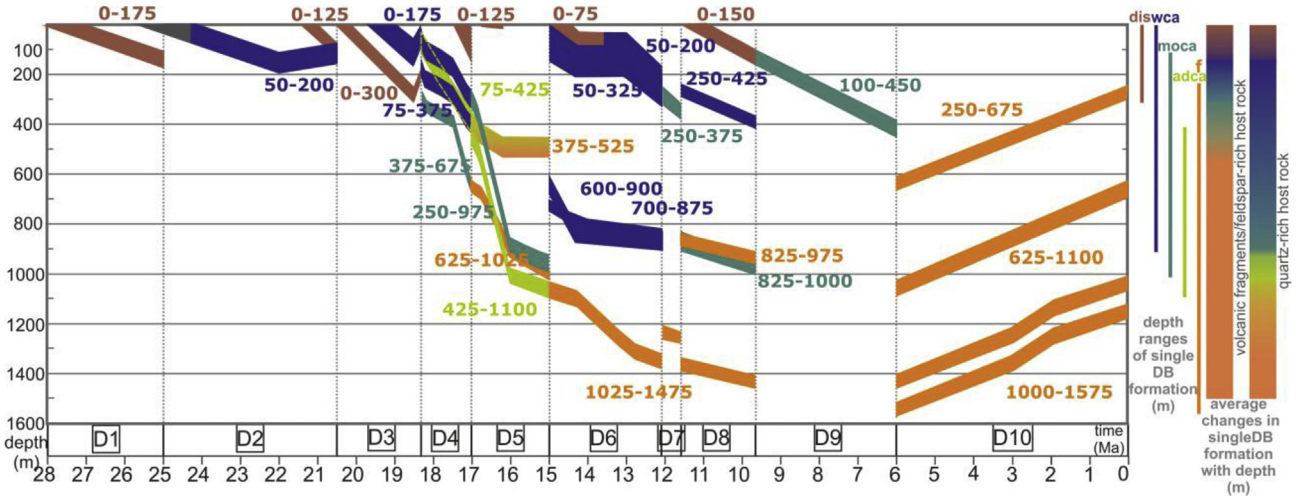

Fig. 10. Summary of the depth ranges of deformation mechanisms in DB types.

poorly constrained (e.g., Wi: ~2–3 Ma).

Based on the burial history disaggregation bands (dis) could form from the near surface to 75–175 m depth (with average of 125 m) but poorly constrained depth estimations at Noe may extend the total depth up to 300 m (Fig. 10). This estimated depth interval is less than depths (~300 m for granular flow without grain flaking) proposed by Fossen (2010b) and seems to be independent from deformation phases or lithology. These features mark disaggregation bands as the earliest deformation structures affecting the sediments.

5.2.2. Cataclastic bands

The weakly (wca) and moderately cataclastic (moca) bands belong to subsequent deformation phases with respect to disaggregation bands; the temporal difference could be 2–4 Ma but during the fastest subsidence (at Et) it is only ~1.5 Ma. The only exception is site Sz, where elapsed time between disaggregation and weakly cataclastic bands is at least 10 Ma. The most advanced cataclasis is related to the major D5 syn-rift phase associated with the fastest subsidence of the Pannonian basin.

Subsidence rate has influenced the time span elapsed during progressive development of cataclasis. In Nógrád area 1.75 ± 1 Ma was enough time for the change from weak to advanced cataclasis. While it could be 4.75 ± 1 Ma and more than 3 Ma in the slowly subsiding Bükk Foreland and Szilvásvárad-Felsőtárkány areas, respectively.

Cataclastic bands could appear from 50 m shallow burial position up to at 1100 m (Fig. 10). In general, the type of cataclasis tends to be more grain destructive as burial depth increases (Fig. 8.). This clear trend is documented by sites with multiple types of cataclastic bands (Sz, An, Bam, Et, Szi). No syn-sedimentary (near surface) cataclasis was observed.

Subsidence curves suggest that depth intervals for weak cataclasis could be ~50–375 m. Alternative classification of Szi-1, -2 bands (see Fig. 9B) to the structural phase of D6 or D8 would extent maximum depth up to 425mwith an average lower value of 250 m across all sites. Moderate cataclasis was found from 100 to 975 m taking the extreme values for individual depth interval estimations. Average depth values would yield a range of 250–620 m. The range of advanced cataclasis is somewhere between ~425 and 1100 m, however, this is only based on two examples giving uncertainty to our estimation. We note that advanced cataclasis is not observed at sites which did not have at least 500–800 m of cover sediments. We speculate the change from moderate to advanced cataclasis could occur around ~800–1000 m. Site A is an outlier for advanced cataclasis as the sample An-4 is the part of decimetre scale DB clustering with tens of bands evolved to outcrop scale fault (Petrik et al., 2014) Therefore this sample is more complex than an individual band.

Weak cataclastic bands from example (Sz) represent a larger formation depth than similar bands in any other sites (Figs. 9 and 10). In other case (Fa) no differences can be detected in the intensity of cataclasis between band sets Fa-1 plus Fa-2 and Fa-3 (Darnó area, see photos in Supplementary 2), although the structural phases (D6 or D8) would imply at least 500 m depth difference (Fig. 9C). We suggest that quartz-rich lithology at D6 and D8 limited more intense cataclasis from a few hundred meters to nearly 800 m depth. In other sites, the feldspar and volcanic glass-rich sandstones (Szi, Nov) promote more efficient cataclastic deformation in shallower depths (~100–450 m) than for quartz-rich bands due to the fragility of volcanic-derived particles. Thus the weaker the host rock grains, the shallower the depth at which cataclastic DB's occurs.

In a few cases, instead of moderate or strong cataclasis, calcite veins or discrete fractures form at relatively shallow (500–600 m) depth (Fig. 10). Our observations show that calcite cementation is the last process, which ceased further DB evolution toward more advanced cataclasis and promoted discrete fracturing at that depth. As cementation results low porosity and stiffness of initially porous sediments, discrete fractures form instead of DBs. Transition from deformation band to discrete fault slip.

5.2.3. Transition from deformation band to discrete fault slip

Although the change of DB formation to discrete fault slip surface is a logical, physically-controlled evolutionary step, an important question is when and at what depth this change could occur. Our observations (Fig. 9) point that no more deformation band can be detected during the post-rift phases within the pre-rift and syn-rift sediments. The change in mechanism is either reflected by reactivations of DBs, (site An, Da), or as ubiquitous occurrence of new faults, joints, veins formed independently from DBs. In DBs the youngest deformation concentrates along a very thin zone, generally asymmetrically on either side of the band. In most cases, the older, conjugate normal DBs bear oblique slickenside lineations demonstrating reactivation in a different stress field. In the studied examples, these discrete structural elements occurred as the youngest deformation phase. In many cases, reactivation of DB surfaces by fault slip occurred during D6-D8 late syn-rift phases. Comparing these phases to burial history (Fig. 9), discrete faults could form at or close to maximum burial.

New discrete faults and joints could occur during the next deformation stage with respect to the last DBs, or the time lag can be large when fractures are post-rift or neotectonic in age. The temporal difference between DB and the oldest discrete fault slip can range from 2.5 ± 1 Ma (Nógrád) up to 3 ± 1.5 Ma (Fa). Multiple fracture sets

developed after DB formation mostly in the Nógrád area which subsided into appropriate depth where cementation may have already started during the mid-Miocene (Fig. 9D.).

The elapsed time between sedimentation and the first occurrence of discrete fracture planes, joints or veins is the largest for the Bükk Foreland area (Fig. 9A) followed by the Nógrád area (Fig. 9D), and the Darnó area (Fig. 9C) (~9, ~7, ~5Ma, respectively). The longest elapsed time can be observed in the Szilvásvárad graben (11 ± 3 Ma) (Fig. 9B). Subsidence rate clearly influence this tendency; the slower the subsidence rate, the longer the time span before discrete faulting begins.

The change from deformation band formation to discrete faulting occurs between 925 and 1475 m in Nógrád area (Figs. 9D), 625–1025 m in the Darnó area (Fig. 9C), and 375–525m in the Bükk Foreland area (Fig. 9A). The latter values are derived from the only sampled clustered DB, where oblique striae on clay smear surface act as a poor constraint on the overall deformation mechanism. In the Darnó area calcite (Fa) and smectite (Da) cement could have significantly decreased porosity and promoted discrete faulting instead of more intense cataclasis. In cases of deeper transition to faulting (Nógrád area), DB formation seems to persist for the largest depth partly due to quartz rich lithology. However, fast subsidence could retard the cementation process, thus rheological conditions remain favourable for band formation. Altogether, these examples indicate that fault evolution from clustered DB could start at burial depths as shallow as ca. 450 m, but single band transition can occur at ~500 ± 100 m in volcanoclastic or feldspar rich and ~1000 ± 100 m in quartz rich host rock, and is ubiquitous from 1100 m (Fig. 10).

5.3. Mineralogy

All the observations on role of mineralogy is in agreement with earlier investigations (Rawling and Goodwin, 2003; Exner and Tschegg, 2012; Lommatzsch et al., 2015) in feldspar-rich sediments.

Our study shows that mineralogy is not so important in near surface or very shallow conditions during disaggregation band formation. In line with burial, volcanic fragment and feldspar dominated host rock display a greater intensity of cataclasis than quartz-rich siliciclastics. Consequently, the role of lithology becomes more pronounced during burial.

5.4. The effect of heterogeneous cementation

Several examples for diagenetic control on local variation in petrophysical properties that affects deformation mechanism are reported in literature (e.g. Eichubl et al., 2004; Torabi and Fossen, 2009; Lommatzsch et al., 2015). Our observations at Noe clearly show that the well-cemented part of the host rock was deformed by calcite veins representing discrete fracture (Fig. 6C), while the continuation of the same structure in the moderately indurated host rock shows advanced cataclasis. In the case of coexisting band and vein formation the deformation mechanism is governed by the local physical properties of host rock determined by diagenesis. A similar situation could occur in site Da where calcite dominoes are parts of advanced cataclastic bands (Petrik et al., 2016). In this site, early diagenetic pore-filling smectite growth could also have reduced porosity and fostered vein formation. In general, calcite cementation seems to have taken place (Szőcs and Hips, 2018) when the fastest subsidence slowed down during later parts of the syn-rift process (Fig. 9). The transition from DB to fault slip or vein formation seems to be gradual across a large depth range.

5.5. Grain size

Silty lithology of site Pe lacks DBs but hosts scratching-type lineation related to frictional slip. In case of alternating lithology, siltstone shows lineation while sandstone hosts DBs (sites An, Ba, Wi). Fine grain size and low primary porosity hampers the formation of DBs. Thus depth ranges for striated siltstones or clays may not offer good lower constraints for DBs (like in site An). On the contrary, despite having a gravelly lithology, at site Sz, the transition from disaggregation to weakly cataclastic types was retarded. As previous studies have shown that larger grain sized lithologies should be more sensitive to grain crushing at increasing depth (Zhang et al., 1990; Schultz et al., 2010). Based on our observations, quartzite-rich composition seems to be a more important factor than (gravelly) grain size in cataclasis intensity.

6. Conclusions

The detailed structural and petrographic observations of DBs in 16 Pannonian Basin sites revealed cohesive conclusions for the temporal evolution of deformation mechanisms and permitted depth scaling of these mechanisms in the context of burial history.

We conclude that:

1) Disaggregation bands are the earliest structures occurring between 0 and 125 m depth and within 3 Ma time span with respect to the deposition of the host sedimentary unit. In partially cemented host rocks the DBs are cemented with calcite or ferruginous cement acting as barrier in the present day situation.
2) Weakly cataclastic band generally appear as the subsequent structure after disaggregation bands forming from very shallow depth (~50 m) until around 800 ± 100 m in quartz rich lithology. This DB type behaves as conduits for the fluid flow and resulted in massive calcite cementation in partially cemented sediments.
3) The transition of weak and moderate cataclasis can be approximately 300 ± 100 m for feldspar or fragile tuffitic components rich host rock and around 900 ± 100 m m in case of quartz-rich sediments. There is one example from clustered DB's where advanced cataclasis with extended quartz comminution could have initiated from around ~250 ± 175 m however the majority of samples suggest almost 1 km burial depth is required for advanced cataclasis to take place.
4) We suggest that burial diagenesis is a key process that promotes discrete faulting at shallower depth than expected. Cementation - partly as a result of regional fluid migration along pre-existing DB- could interrupt the DB evolution resulting in coexisting DB formation and calcite veining from ~425 to 1000 m burial depth. In general, the discrete fault planes on the margin of moderately or advancedly cataclastic bands and the formation of new fracture planes generally started from ~500 ± 100 m in volcanoclastic or feldspar rich host rocks, and 1000 ± 100 m in quartz-rich host rocks.
5) No more deformation band formation is detected during the post-rift phases within the pre-rift and syn-rift sediments.
6) Comparative examples from variable lithology revealed that mineralogy is not so important in near surface or very shallow conditions during disaggregation band formation. However, the role of lithology becomes more pronounced during burial. Shallowly buried volcanic fragment and feldspar dominated host rock display a greater intensity of cataclasis than quartz-rich siliciclastics.
7) The combined methodology demonstrated in this paper can be used for calibrating DB formation depths in other sedimentary basins including those with different lithology (e.g., calcarenite, volcanoclastics) and with variable strain rates and predict potential role of DB types in fluid migration with depth.

Acknowledgments

The research was supported by Hungarian Scientific Research Fund (NKFIH OTKA) 83150 and 113013. Anna Swierczewska and Antoni Tokarski (Kraków) participated in the early field work and discussions. We thank all reviewers for their constructive comments.

Appendix A. Supplementary data

Supplementary data to this article can be found online at https://doi.org/10.1016/j.marpetgeo.2019.04.006.

References

Anderson, E.M., 1951. The Dynamics of Faulting and Dyke Formation with Application to Britain, second ed. Oliver & Boyd, Edinburgh, pp. 206.

Angelier, J., 1984. Tectonic analysis of fault slip data sets. J. Geophys. Res. 89 (B7), 5835–5848.

Angelier, J., Manoussis, S., 1980. Classification automatique et distinction des phases superposée en tectonique de failles. C. R. Acad. Sci. 290 (série D), 651–654 Paris.

Antonellini, M.A., Pollard, D.D., 1995. Distinct element modeling of deformation bands in sandstone. J. Struct. Geol. 17 (8), 1165–1182.

Arató, R., Dunkl, I., Takács, Á., Szebényi, G., Gerdes, A., von Eynatten, H., 2019. Thermal evolution in the exhumed basement of a stratovolcano: case study of the Miocene Mátra Volcano, Pannonian Basin. J. Geol. Soc. 175 (5), 820–835.

Aydin, A., 1978. Small faults formed as deformation bands in sandstone. Pure Appl. Geophys. 116, 913–930.

Aydin, A., Borja, R.I., Eichhubl, P., 2006. Geological and mathematical framework for failuremodes in granular rock. J. Struct. Geol. 28, 83–98.

Balázs, A., Matenco, L., Magyar, I., Horváth, F., Cloetingh, S., 2016. The link between tectonics and sedimentation in back-arc basins: new genetic constraints from the analysis of the Pannonian Basin. Tectonics 35, 1526–1559. https://doi.org/10.1002/2015TC004109.

Báldi, T., 1986. Mid-Tertiary Stratigraphy and Paleogeographic Evolution of Hungary. Akadémia Press, Budapest, pp. 201.

Ballas, G., Soliva, R., Sizun, J.-P., Fossen, H., Benedicto, A., Skurtveit, E., 2013. Shear-enhanced compaction bands formed at shallow burial conditions; implications for fluid flow (Provence, France). J. Struct. Geol. 47, 3–15.

Ballas, G., Soliva, R., Benedicto, A., Sizun, J.P., 2014. Control of tectonic setting and large-scale faults on the basin-scale distribution of deformation bands in porous sandstone (Provence, France). Mar. Petrol. Geol. 55, 142–159.

Balsamo, F., Storti, F., Piovano, B., Salvini, F., Cifelli, F., Lima, C., 2008. Time dependent structural architecture of subsidiary fracturing and stress pattern in the tip region of an extensional growth fault system. Tarquinia Basin Italy: Tectonophy. 454, 54–69.

Beke, B., 2016. The Role of Deformation Bands in Cenozoic Structural Evolution of Northern Hungary. [Ph.D. thesis]. Eötvös Loránd University, Budapest, pp. 148.

Beke, B., Fodor, L., 2014. Deformation band in porous media. Foldtani Kozlony 144, 255–274.

Bergerat, F., Geyssant, J., Lepvrier, C., 1984. Neotectonic outline of the Intra-Carpathian basins in Hungary. Acta Geol. Hung. 27, 237–251.

Bernabé, Y., Fryer, D.T., Hayes, J.A., 1992. The effect of cement on the strength of granular rocks. Geophys. Res. 19 (14), 1511–1514.

Blanckenburg, F., Kagami, H., Deautsch, A., Wiedenbeck, M., Oberli, F., Meier, M., Barth, S., Fischer, H., 1998. The origin of Alpine plutons along the Periadriatic Lineament: S chweizerische Mineralogische und Petrographische. Mitteilungen 78, 55–66.

Cashman, S., Cashman, K., 2000. Cataclasis and deformation-band formation in unconsolidated marine terrace sand. Humboldt County California: Geol. 28, 111–114.

Cheung, C.S., Baud, P., Wong, T.F., 2012. Effect of grain size distribution on the development of compaction localization in porous sandstone. Geophys. Res. Lett. 39, L21302.

Csontos, L., 1999. Structural outline of the Bükk mts (N Hungary). Foldtani Kozlony 129 (4), 611–651.

Csontos, L., Nagymarosy, A., 1998. The Mid-Hungarian line: a zone of repeated tectonic inversions. Tectonophysics 297, 51–71.

Davatzes, N.C., Aydin, A., 2003. Overprinting faulting mechanisms in high porosity sandstones of SE Utah. J. Struct. Geol. 25, 1795–1813.

Davatzes, N.C., Eichhubl, P., Aydin, A., 2005. Structural evolution of fault zones in sandstone by multiple deformation mechanisms: moab fault, southeast Utah. Geol. Soc. Am. Bull. 117, 135–148.

Dunkl, I., Árkai, P., Balogh, K., Csontos, L., Nagy, G., 1994. Thermal modelling based on apatite fission track dating: the uplift history of the Bükk Mts. Bull. Hungarian Geol. Soc. 124 (1), 1–24 (in Hungarian).

Engelder, T., 1974. Cataclasis and the generation of fault gouge. Geol. Soc. Am. Bull. 85, 1515–1522.

Eichhubl, P., Taylor, W.L., Pollard, D.D., Aydin, A., 2004. Paleo-fluid flow and deformation in the Aztec Sandstone at the Valley of Fire, Nevada-evidence for the coupling of hydrogeologic, diagenetic, and tectonic processes. Geol. Soc. Am. Bull. 116, 1120–1136.

Exner, U., Tschegg, C., 2012. Preferential cataclastic grain size reduction of feldspar in deformation bands in poorly consolidated arkosic sands. J. Struct. Geol. 43, 63–72.

Fodor, L., Jelen, B., Márton, E., Skaberne, D., Čar, J., Vrabec, M., 1998. Miocene-Pliocene tectonic evolution of the Slovenian Periadriatic Line and surrounding area – implication for Alpine-Carpathian extrusion models. Tectonics 17, 690–709.

Fodor, L., Csontos, L., Bada, G., Györfi, I., Benkovics, L., 1999. Tertiary tectonic evolution of the Pannonian basin system and neighbouring orogens: a new synthesis of paleostress data. In: In: Durand, B., Jolivet, L., Horváth, F., Séranne, M. (Eds.), The Mediterranean Basins: Tertiary Extension within the Alpine Orogen: London, vol 156. Geological Society, Special Publication, pp. 295–334.

Fodor, L., Radócz, Gy, Sztanó, O., Koroknai, B., Csontos, L., Harangi, Sz, 2005. Post-conference excursion: tectonics, sedimentation and magmatism along the Darnó zone. Geolines 19, 142–162.

Fossen, H., 2010a. Deformation bands formed during soft-sediment deformation: observations from SE Utah. Mar. Petrol. Geol. 27, 215–222.

Fossen, H., 2010b. Deformation at the microscale in fossen. In: H (Ed.), Structural Geology. Cambridge University Press, New York, pp. 203–216.

Fossen, H., Schultz, R., Shipton, Z., Mair, K., 2007. Deformation bands in sandstone – a review. J. Geol. Soc. Lond. 164, 755–769.

Fossen, H., Soliva, R., Ballas, G., Trzaskos, B., Cavalcante, G.C., Schultz, R.A., 2017. A Review of Deformation Bands in Reservoir Sandstones: Geometries, Mechanisms and Distribution, vol 459. Geological Society, Special Paper, pp. 9–33.

Haas, J., Budai, T., Csontos, L., Fodor, L., Konrád, Gy, 2010. Pre-Cenozoic Geological Map of Hungary, Scale 1:500 000. Geological and Geophysical Institute of Hungary scale 1: 500 000, 1 sheet.

Hámor, G., 1985. Geology of the nógrád–cserhát area: budapest. Geol. Hung. Ser. Geol. 22, 307.

Harangi, Sz, 2001. Neogene to quaternary volcanism of the carpathian-pannonian region - a review. Acta Geol. Hung. 44, 223–258.

Hesthammer, J., Fossen, H., 2001. Structural core analysis from the Gullfaks area, northern North Sea. Mar. Petrol. Geol. 18, 411–439.

Hohenegger, J., Ćorić, S., Wagreich, M., 2014. Timing of the middle Miocene badenian stage of the central paratethys. Geol. Carpathica 65, 55–66.

Hodson, K.R., Crider, J.G., Huntington, K.W., 2016. Temperature and composition of carbonate cements record early structural control on cementation in a nascent deformation band fault zone: moab Fault, Utah, USA. Tectonophysics 690, 240–252.

Horváth, F., 1995. Phases of compression during the evolution of the Pannonian Basin and its bearing on hydrocarbon exploration. Mar. Petrol. Geol. 12, 837–844.

Horváth, F., Musitz, B., Balázs, A., Végh, A., Uhrin, A., Nádor, A., 2015. Evolution of the Pannonian basin and its geothermal resources. Geothermics 53, 328–352.

Laczó, I., 1982. The Geological Evaluation of Hungarian Vitrinite Reflectance Values: the Annual Report of the Hungarian Geological Institute from 1982. pp. 417–437 (in Hungarian).

Less, Gy, 2005. Palaeogene. In: Pelikán, P., Budai, T. (Eds.), Geology of the Bükk: Budapest. Geological Institute of Hungary, pp. 204–211 ISBN 963 671 253 0.

Less, Gy, Frijia, G., 2015. New Sr-isotope ages from the central parathetys. In: Hungarian Paleontological Assembly, 18th, Field Guide, pp. 19–20.

Less, Gy, Mello, J., 2004. Geological Map of the Gemer-Bükk Area. Geological Institute of Hungary scale 1:100.000, 1 sheet.

Less, Gy, Gulácsi, Z., Kovács, S., Pelikán, P., Pentelényi, L., Rezessy, A., Sásdi, L., 2005. Geological Map of the Bükk Mountains Geological Institute of Hungary scale 1:50.000, 1 sheet.

Littke, R., Büker, C., Lückge, A., Sachsenhofer, R.F., Welte, D.H., 1994. A new evaluation of paleo-heat flows and eroded thicknesses for the Carboniferous Ruhr Basin, western Germany. Int. J. Coal Geol. 26, 155–183.

Lommatzsch, M., Exner, U., Gier, S., Grasemann, B., 2015. Structural and chemical controls of deformation bands on fluid flow: interplay between cataclasis and diagenetic alteration. AAPG (Am. Assoc. Pet. Geol.) Bull. 99, 698–710.

Lukács, R., Harangi, S., Guillong, M., Bachmann, O., Fodor, L., Buret, Y., Dunkl, I., Sliwinski, J., von Quadt, A., Peytcheva, I., Zimmerer, M., 2018. Early to Mid-Miocene syn-extensional massive silicic volcanism in the Pannonian Basin (East-Central Europe): eruption chronology, correlation potential and geodynamic implications. Earth Sci. Rev. 179, 1–19.

Magyar, I., Radivojević, D., Sztanó, O., Synak, R., Ujszászi, K., Pócsik, M., 2013. Progradation of the paleo-danube shelf margin across the Pannonian basin during the late Miocene and early pliocene. Glob. Planet. Chang. 103, 168–173.

Mair, K., Main, I., Elphick, S., 2000. Sequential growth of deformation bands in the laboratory. J. Struct. Geol. 22, 25–42.

Márton, E., Fodor, L., 1995. Combination of paleomagnetic and stress data — a case study from North Hungary. Tectonophysics 242, 99–114.

Müller, W., Prosser, G., Mancktelow, N., Villa, I.M., Kelly, S.P., Viola, G., Oberli, F., 2001. Geochronological constraints on te evolution of the Periadriatic fault system (Alps). Int. J. Earth Sci. 90, 623–653.

Nagymarosy, A., 1990. Paleogeographical and paleotectonical outlines of some Intracarpathian Paleogene basins. Geol. Zb. - Geol. Carpathica 41, 259–274.

Palotai, M., Csontos, L., 2010. Strike-slip reactivation of a Palaeogene to Miocene fold and thrust belt along the central part of the Mid-Hungarian Shear Zone. Geol. Carpathica 61 (6), 483–493.

Pelikán, P., Less, Gy, Kovács, S., Pentelényi, L., Sásdi, L., 2005. Geology of the Bükk Mountains. Explanatory Book to the Geological Map of the Bükk Mountains, 1:50.000. Geological Institute of Hungary, pp. 284 ISBN 963 671 253 0.

Petrik, A., Beke, B., Fodor, L., 2014. Combined analysis of faults and deformation bands reveals the Cenozoic structural evolution of the southern Bükk foreland (Hungary). Tectonophysics 633, 43–62.

Petrik, A., Beke, B., Fodor, L., Lukács, R., 2016. Cenozoic structural evolution of the southwestern Bükk Mts. and the southern part of the Darnó Deformation Belt (NE Hungary). Geol. Carpathica 67 (1), 83–104.

Pomella, H., Stipp, M., Fügenschuh, B., 2012. Thermochronological record of thrusting and strike-slip faulting along the Giudicarie fault system (Alps, Northern Italy). Tectonophysics 579, 118–130.

Püspöki, Z., Makk-Tóth, Á., Kozák, M., Dávid, Á., McIntosh, R., Buday, T., Demeter, G., Kiss, J., Terebesi-Püspöki, M., Barta, K., Csordás, Cs, Kiss, J., 2009. Truncated higher order sequences as responses to compressive intraplate tectonic events on eustatic sea-level rise. Sediment. Geol. 219, 208–236.

Rawling, G.C., Goodwin, L.B., 2003. Cataclasis and particulate flow in faulted, poorly lithified sediments. J. Struct. Geol. 25, 317–331.

Rotevatn, A., Torabi, A., Fossen, H., Braathen, A., 2008. Slipped deformation bands: a new type of cataclastic deformation bands in Western Sinai, Suez rift, Egypt. J. Struct. Geol. 30, 1317–1331.

Royden, F., Horváth, F., Burchfiel, B.C., 1982. Transform faulting, extension and subduction in the Carpathian Pannonian region. Geol. Soc. Am. Bull. 93 (8), 717–725.
Ruszkiczay-Rüdiger, Zs, Fodor, L.I., Horváth, E., 2007. Neotectonics and quaternary landscape evolution of the gödöllő hills, central Pannonian basin, Hungary. Glob. Planet. Chang. 58 (1–4), 181–196.
Sant, K., Kirscher, U., Reichenbacher, B., Pippèrr, M., Jung, D., Doppler, G., Krijgsman, W., 2017. Late Burdigalian sea retreat from the North Alpine Foreland Basin: new magnetostratigraphic age constraints. Glob. Planet. Chang. 152, 38–50.
Schmid, S.M., Aebli, H.R., Heiler, F., Zingg, A., 1989. The role of the Periadriatic line in the Tectonic evolution of the Alps. In: In: Coward, M.P., Dietrich, D., Park, R.G. (Eds.), Alpine Tectonics, vol 45. Geological Society Special Publication, London, pp. 153–171 1.
Schmid, S.M., Fügenschuh, B., Kissling, E., Schuster, R., 2004. Tectonic map and overall architecture of the Alpine orogen. Eclogae Geol. Helv. 97, 93–117.
Schultz, R.A., Siddharthan, R., 2005. A general framework for the occurrence and faulting of deformation bands in porous granular rocks. Tectonophysics 411 (1), 1–18.
Schultz, R.A., Okubo, C.H., Fossen, H., 2010. Porosity and grain size controls on compaction band formation in Jurassic Navajo Sandstone. Geophys. Res. Lett. 37, 1–5.
Soliva, R., Ballas, G., Fossen, H., Philit, S., 2016. Tectonic regime controls clustering of deformation bands in porous sandstone. Geology 44 (6), 423–426. https://doi.org/10.1130/G37585.1.
Szakács, A., Zelenka, T., Márton, E., Pécskay, Z., Póka, T., 1998. Miocene acidic explosive volcanism in the Bükk Foreland, Hungary: identifying eruptive sequences and searching for source locations. Acta Geol. Hung. 41 (4), 413–435.
Szőcs, E., Hips, K., 2018. Multiphase carbonate cementation in the Miocene Pétervására Sandstone (North Hungary): implications for basinal fluid flow and burial history. Geol. Carpathica 69 (6), 515–527.
Sztanó, O., 1994. The Tide-Influenced Pétervására Sandstone, Early Miocene, Northern Hungary: Sedimentology, Paleogeography and Basin Development. [Ph.D thesis]. Utrecht, University of Utrecht, pp. 155.
Sztanó, O., 1995. Palaeogeographic significance of tidal deposits: an example from an early Miocene Paratethys embayment, Northern Hungary. Palaeogeogr. Palaeoclimatol. Palaeoecol. 113 (2), 173–187.
Sztanó, O., Józsa, S., 1996. Interaction of basin-margin faults and tidal currents on nearshore sedimentary architecture and composition: a case study from the Early Miocene of northern Hungary. Tectonophysics 266 (1), 319–341.
Sztanó, O., Tari, G., 1993. Early Miocene basin evolution in northern Hungary: tectonics and eustasy. Tectonophysics 226 (1), 485–502.
Tari, G., 1988. Strike-slip origin of the Vatta-Maklár trough. Acta Geol. Hung. 31, 101–109.
Tari, G., Horváth, F., Rumpler, J., 1992. Styles of extension in the Pannonian basin. Tectonophysics 208, 203–219.
Tari, G., Báldi, T., Báldi-Beke, M., 1993. Paleogene retroarc flexural basin beneath the Neogene Pannonian Basin: a geodynamic model. Tectonophysics 226, 433–455.
Torabi, A., Fossen, H., 2009. Spatial variation of microstructure and petrophysical properties along deformation bands in reservoir sandstones. AAPG (Am. Assoc. Pet. Geol.) Bull. 93, 919–938.
Vass, D., 2002. Unique Cenozoic lithofacies in the northern part of the Darnó Fault Belt and its surroundings: an overview. Acta Geol. Hung. 45, 79–99.
Zelenka, T., Baksa, Cs, Balla, Z., Földessy, J., Járányi-Földessy, K., 1983. Is the Darnó line a mesozoic paleogeographical boundary? Bull. Hungarian Geol. Soc. 113, 27–37.
Zhang, J., Wong, T.F., Davis, D.M., 1990. Micromechanics of pressure-induced grain crushing in porous rocks. J. Geophys. Res. 95, 341–352.